Anthony C. Harris · Charlotte M. Allen
Scott E. Bryan · Ian H. Campbell
Rodney J. Holcombe · J. Michael Palin

ELA-ICP-MS U–Pb zircon geochronology of regional volcanism hosting the Bajo de la Alumbrera Cu–Au deposit: implications for porphyry-related mineralization

Abstract ELA-ICP-MS U–Pb zircon geochronology has been used to show that the porphyritic intrusions related to the formation of the Bajo de la Alumbrera porphyry Cu–Au deposit, NW Argentina, are cogenetic with stratigraphically well-constrained volcanic and volcaniclastic rocks of the Late Miocene Farallón Negro Volcanic Complex. Zircon geochronology for intrusions in this deposit and the host volcanic sequence show that multiple mineralized porphyries were emplaced in a volcanic complex that developed over 1.5 million years. Volcanism occurred in a multivent volcanic complex in a siliciclastic intermontane basin. The complex evolved from early mafic-intermediate effusive phases to a later silicic explosive phase associated with mafic intrusions. Zircons from the basal mafic-intermediate lavas have ages that range from 8.46±0.14 to 7.94±0.27 Ma. Regionally extensive silicic explosive volcanism occurred at ~8.0 Ma (8.05±0.13 and 7.96±0.11 Ma), which is co-temporal with intrusion of the earliest mineralized porphyries at Bajo de la Alumbrera (8.02±0.14 and 7.98±0.14 Ma). Regional uplift and erosion followed during which the magmatic-hydrothermal system was probably unroofed. Shortly thereafter, dacitic lava domes were extruded (7.95±0.17 Ma) and rhyolitic diatremes (7.79±0.13 Ma) deposited thick tuff blankets across the region. Emplacement of large intermediate composition stocks occurred at 7.37±0.22 Ma, shortly before renewed magmatism occurred at Bajo de la Alumbrera (7.10±0.07 Ma). The latest porphyry intrusive event is temporally associated with new ore-bearing magmatic-hydrothermal fluids. Other dacitic intrusions are associated with subeconomic deposits that formed synchronously with the mineralized porphyries at Bajo de la Alumbrera. However, their emplacement continued (from 7.10± 0.06 to 6.93±0.07 Ma) after the final intrusion at Bajo de al Alumbrera. Regional volcanism had ceased by 6.8 Ma (6.92±0.07 Ma).

The brief history of the volcanic complex hosting the Bajo de la Alumbrera Cu–Au deposit differs from that of other Andean provinces hosting porphyry deposits. For example, at the El Salvador porphyry copper district in Chile, magmatism related to Cu mineralization was episodic in regional igneous activity that occurred over tens of millions of years. Bajo de la Alumbrera resulted from the superposition of multiple porphyry-related hydrothermal systems, temporally separated by a million years. It appears that the metal budget in porphyry ore deposits is not simply a function of their longevity and/or the superposition of multiple porphyry systems. Nor is it a function of the duration of the associated cycle of magmatism. Instead, the timing of processes operating in the parental magma body is the controlling factor in the formation of a fertile porphyry-related ore system.

Keywords Copper · Gold · Lava domes · Porphyry · U–Pb geochronology

A. C. Harris (&) · S. E. Bryan · R. J. Holcombe
Department of Earth Sciences,
The University of Queensland, 4072 Brisbane, Australia
E-mail: A.Harris@utas.edu.au
Fax: +61 3 6226 7662

C. M. Allen · I. H. Campbell · J. M. Palin
Research School of Earth Sciences,
Australian National University, 2006 Canberra, Australia

Present address: A. C. Harris
Centre for Ore Deposit Research and School of Earth Sciences,
University of Tasmania, 7001 Hobart, Australia

Present address: J. M. Palin
Department of Geology, University of Otago,
9001 Dunedin, New Zealand

Introduction

For most porphyry ore deposits, very little is known about the host volcanic architecture and the exact timing and relationship to volcanism because the associated intrusions generally lack coeval volcanic and co-magmatic rocks. Porphyry Cu deposits form from huge hydrothermal systems centered on small porphyritic intrusions that are assumed to be apophyses to larger plutons. Hydrothermal alteration develops from early potassic through to late phyllic alteration. High-temperature, saline magmatic fluids are responsible for the potassic (quartz–biotite–K-feldspar) assemblages, while phyllic alteration (quartz–sericite ± pyrite) develops as the magmatic–hydrothermal fluid cools and/or mixes with low salinity, lower temperature meteoric waters (e.g., Hedenquist and Richards 1998).

The low closure temperature of the most commonly analyzed minerals (i.e., biotite and sericite) prevents the high-temperature geochronology of these deposits being determined using the K–Ar or $^{40}Ar/^{39}Ar$ techniques (see McDougall and Harrison 1999). U–Pb zircon geochronology has confirmed that the magmatic history is characterized by multiple intrusions in the larger deposits (e.g., Cornejo et al. 1997; Reynolds et al. 1998; Ballard et al. 2001). New ELA-ICP-MS U–Pb zircon geochronology of the Bajo de la Alumbrera porphyry Cu–Au deposit, NW Argentina (402 · 10^6 t of ore averaging 0.54% Cu and 0.64 g/t Au, D. Keough personal communication 2001), reveals that hydrothermal alteration developed around at least two distinct porphyry intrusions, emplaced a million years apart. When combined with previously reported $^{40}Ar/^{39}Ar$ ages (Sasso and Clark 1998) the new data suggest that hydrothermal alteration probably occurred at least for a few hundred thousand years.

This new ELA-ICP-MS U–Pb zircon geochronology study also suggests that the temporal evolution of the Farallón Negro Volcanics may differ from that of other porphyry provinces, where the emplacement of intrusions related to a porphyry ore deposit occurs following a protracted period of regional magmatism (e.g., Marsh et al. 1997). Here early mineralization immediately followed the onset of volcanism or occurred within 500,000 years. This implies that the fertility of the parental magma is not always dependent on a long-lived history (e.g., Skewes and Stern 1995; Cornejo et al. 1997; Marsh et al. 1997).

Geological setting

The Farallón Negro district is in NW Argentina, at latitude 27°15'S, longitude 66°33'W (Fig. 1), and at an average altitude of 2.60 km above sea level. The district geology is an intermontane basin occurring within the northeast-trending Tucuman Fault Zone (TFZ; de Urreiztieta et al. 1996). The TFZ is a linear deformation zone that marks the boundary between the Puna-Altiplano to the north and the Sierras Pampeanas in the south (Fig. 1).

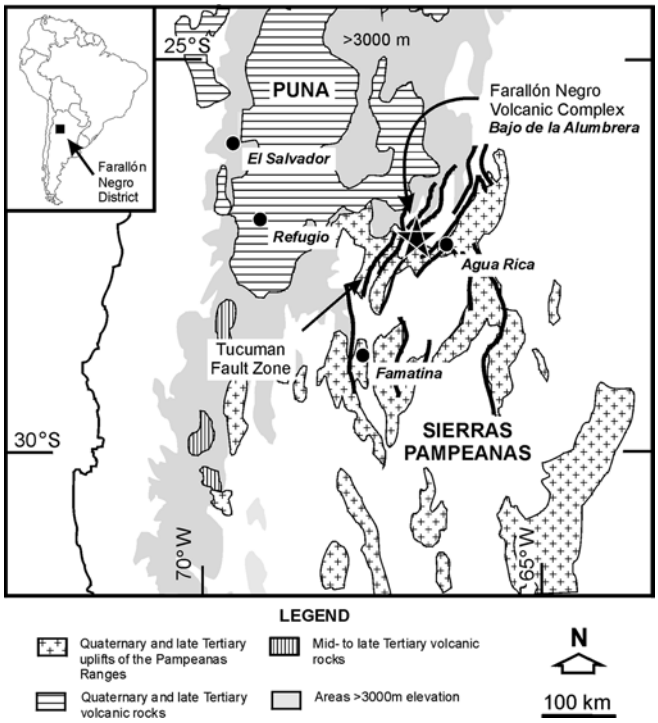

Fig. 1 Physio-tectonic map of the central Andes showing the location of the Farallón Negro Volcanic Complex, in which the Bajo de la Alumbrera porphyry Cu–Au deposit occurs. The complex was emplaced ~200 km east of the main Miocene arc. The Farallón Negro district is an intermontane basin in the Tucuman Fault Zone (TFZ); i.e., the fault zone that marks the transition between the Puna-Altiplano to the north and the Sierras Pampeanas to the south. After Jordan et al. (1983). Ore deposits (circles) are also annotated

The Puna-Altiplano is a plateau, 700 km long and 200 km wide, with an average elevation of 3.65 km above sea level. The Sierras Pampeanas of NW Argentina is a deep-seated, actively contracting (Smalley 1996) basement-uplift terrane (Jordan et al. 1983; Jordan and Allmendinger 1986), in which the Bajo de la Alumbrera deposit occurs. Uplift of crystalline basement blocks occurred during the Middle Miocene and continued intermittently to the Recent (Jordan and Allmendinger 1986; Reynolds et al. 1987; Tabbutt et al. 1987; Ramos et al. 1988; Strecker et al. 1989, 1990; Tabbutt 1990; Coughlin et al. 1998). Magmatism in the Farallón Negro district is temporally related to a Miocene orogenic event that began with the uplift of the Puna-Altiplano, and ended with the closure of the intermontane basin during the Late Miocene–Pliocene uplift of the Sierras Pampeanas (Sasso and Clark 1998).

Llambías (1972) first related the andesitic rocks of the Farallón Negro district (Fig. 2) to a large stratovolcano. Sillitoe (1973) expanded this concept, inferring that the stratovolcano occurred immediately above the Bajo de la Alumbrera porphyry Cu–Au deposit. This model,

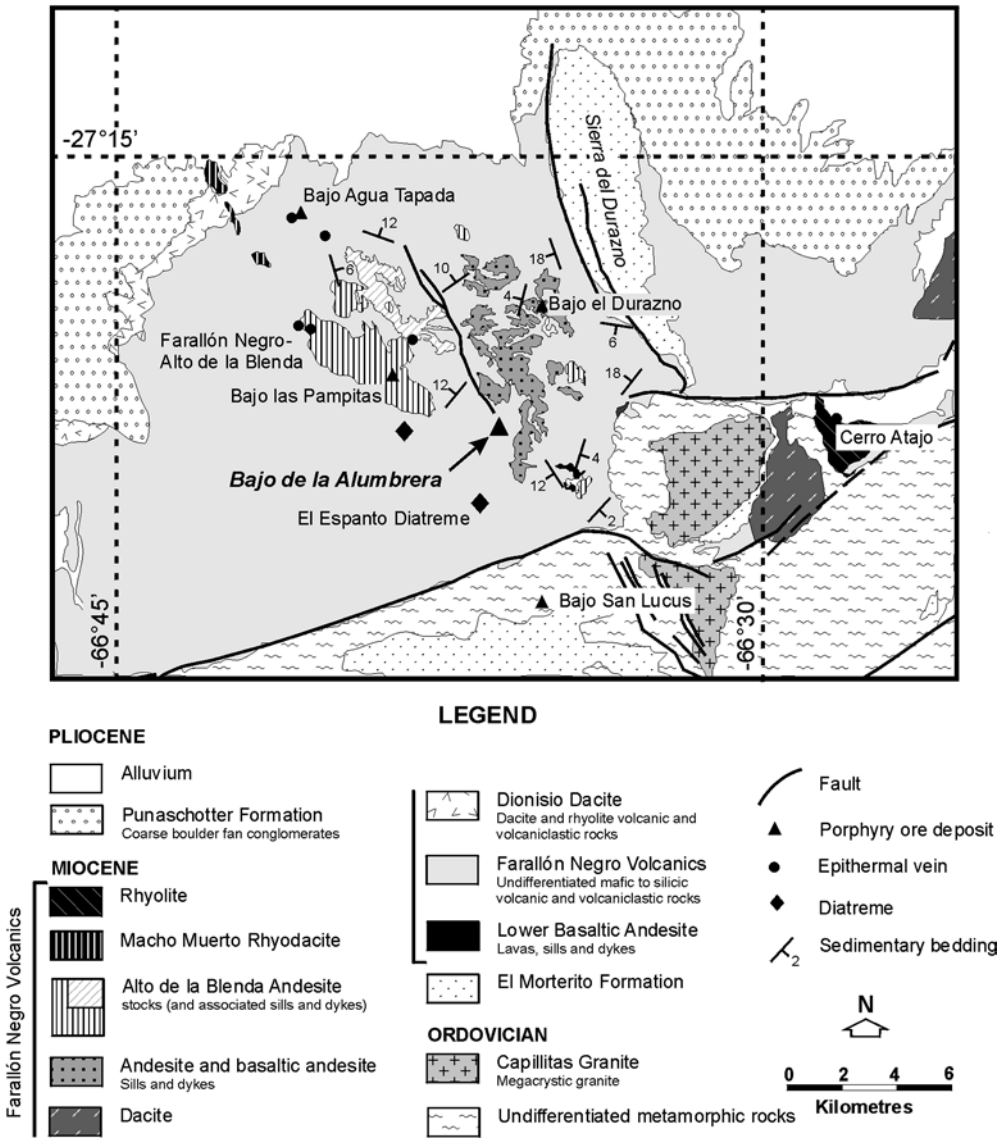

Fig. 2 Generalized geologic map of the Farallón Negro district, NW Argentina (after Sasso 1997; Proffett 1997; and incorporates new mapping data), showing the locations of deposits and mineral occurrences cited in text. The map has annotated bedding measurements summarized from new and unpublished mapping data. Note that although there are perturbations, the stratigraphy generally dips towards the northwest. Previous studies of the Farallón Negro Volcanic Complex have not recognized lateral up-sequence change in the stratigraphy from SE to the N and NW, instead correlating similar lithologies on either side of the district (e.g., Proffett 1997). In addition, the rocks exposed around Bajo de la Alumbrera are dominated by andesite and basaltic andesite sills and dykes, thus obscuring the early volcanic stratigraphy

however, was based on only sparse field data. Proffett (1995, 1997) refined this model with detailed mapping around Bajo de la Alumbrera. He proposed that the andesite volcanic rocks of the district formed the flanks of a large stratovolcano (25 km in diameter and 4 km high), where the porphyry ore deposit occurred on the eastern flank (Proffett 1997; J.M. Proffett, written communication 2001).

A new stratigraphy (Fig. 3; Harris 2002) has established a predominance of sedimentary lithofacies and the recurrence of fine-grained sandstone and siltstone intervals with massive basaltic andesite and andesite breccias, which must have been wet during regional volcanism as they host peperitic intrusions. Overall, field observations indicate that volcanism and related volcaniclastic sedimentation occurred within a large, active sedimentary basin. The sedimentary rocks had multiple sources, as evident from proximal lava facies, interstratification of proximal and more distal volcanic lithofacies, and the coarse grain-size and clast angularity of the polymictic sedimentary breccias. The earliest phases of sedimentation occurred in an unconfined alluvial environment dominated by sheet-flood and debris-flow processes. However, during emplacement of more silicic lava domes in the latter part of the eruptive history, areas of depression formed between the domes producing localized ephemeral lacustrine environments.

Historically, the Farallón Negro Volcanic Complex is best known as host to the Bajo de la Alumbrera porphyry Cu–Au deposit. Exploration and mining over the

c

Fig. 3 Generalized composite stratigraphic section of the volcanic and volcaniclastic sequence of the Farallón Negro Volcanic Complex. Complied from 18 km of measured sections and 1:10,000-scale mapping of a large part of the Farallón Negro Volcanic Complex (Harris 2002). Note that the vertical is not to a fixed scale and horizontal scale is grain size: f fine, m medium, c coarse, vc very coarse. Included are the U–Pb zircon ages for significant volcanic and subvolcanic intrusions (see text for unit descriptions)

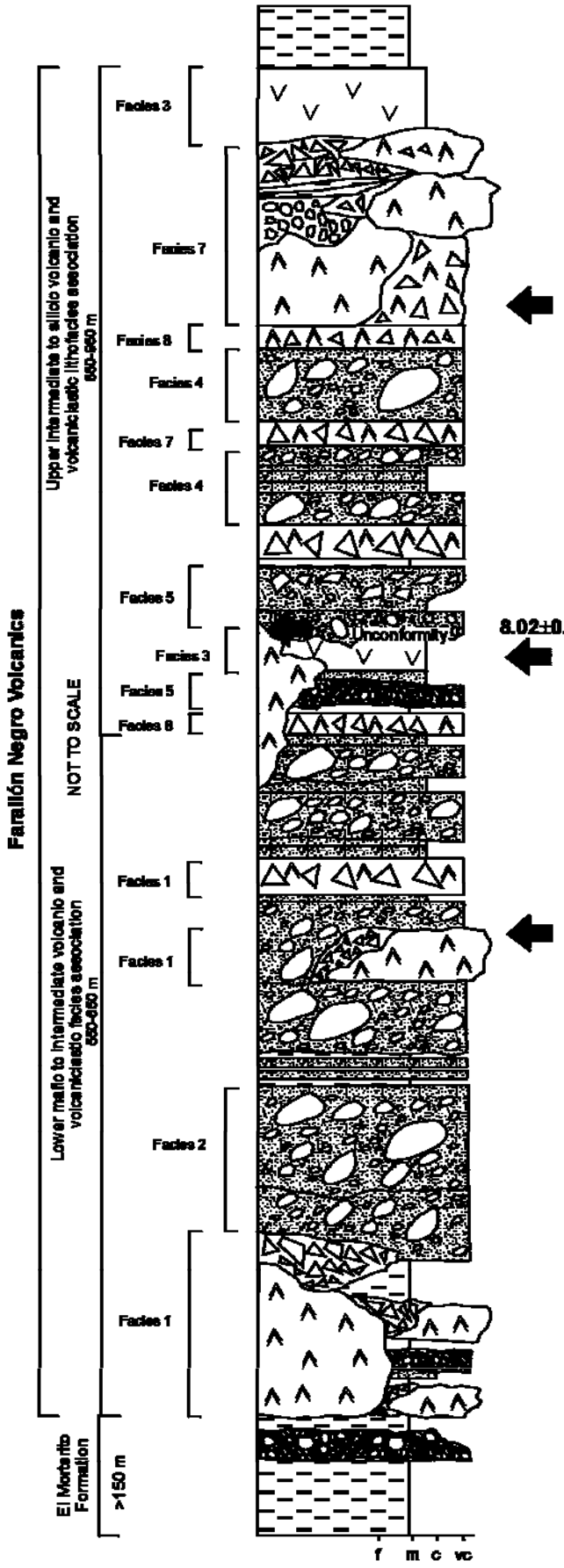

Red brown mica siltstone and thin-bedded, sorted coarse to fine-grained feldspar-lithic (quartz) sandstone.

Bedded rhyolitic ash and lapilli sandstone interpreted as a phreatomagmatic base surge and fallout deposit.

Coarse-grained hornblende-(biotite) plagioclase-phyric andesite to dacite lava domes and block-and-ash deposit.

Thin laminar red siltstones and fine sandstones.

Non stratified dacitic and andesitic breccia. Ragged and fibrous margins to clasts of a near monomict breccia, where the matrix and the clast composition is similar coarse-grained hornblende and plagioclase phyric dacite to andesite.

7.95±0.17 Ma - Dionisio Dacite

Bedded boulder and pebble conglomerates with red laminar siltstone.

Non stratified coarse grained hornblende-plagioclase-phyric andesite breccias interpreted as block-and-ash deposits.

Basement clasts

8.02±0.14 Ma; 7.98±0.14 Ma - Alumbrera Dacite

8.05±0.13 Ma; 7.96±0.11 Ma - La Josefa Tuff

Bedded rhyolitic ash and lapilli sandstone interpreted as a phreatomagmatic base surge and fallout deposit.

Basement clasts

Coarse-grained hornblende plagioclase (biotite)-phyric andesite peperitic intrusives.

Coarse-grained polymictic sedimentary breccias interbedded with massive hornblende-plagioclase-rich ash to lapilli sandstone.

Non stratified coarse grained hornblende-plagioclase-phyric andesite breccias.

8.46±0.14 Ma; 7.94±0.27 Ma - Lower Basaltic Andesite (Durazno Andesite)

Coarse-grained pyroxene-plagioclase phyric basaltic andesite lavas and autobreccias.

Bedded sedimentary breccias. Polymict matrix-supported breccia angular to subrounded plagioclase- and pyroxene-phyric andesitic volcanic clasts set in coarse plagioclase lithic sandstone matrix. Cross laminated sandstones form the base to most reverse graded beds. Thin red brown siltstone and fine sandstone partings occur on the upper surface of the more massive breccia beds.

Non stratified coarse grained pyroxene-plagioclase-phyric basalt and basaltic andesite breccias.

Coarse grained pyroxene-plagioclase-phyric basalt and basaltic andesite peperitic sills, dykes and lavas.

Well sorted to massive, reverse graded pebble conglomerates, with angular to subrounded plagioclase- phyric and schist clasts set in a coarse-grained lithic feldspar sandstone.

Red brown mica siltstone and thin-bedded, sorted coarse- to fine-grained feldspar-lithic (quartz) sandstone. Sandstone beds have erosive bases and display normal grading. Cross lamination and pebble lags are present on many bedding surfaces. Pebble conglomerate consist of well rounded basement and plagioclase-phyric andesite volcanics.

past 50 years has found a number of smaller, subeconomic porphyry Cu–Au deposits (e.g., Bajo el Durazno, Bajo las Pampitas and Bajo Agua Tapada) and epithermal Au–Ag (Pb–Zn ± Cu) veins (e.g., Farallón Negro-Alto de la Blenda, Morro Bola, La Josefe, and Agua Tapada; Sister 1963; Llambías 1972). Approximately 25 km to the east of the immediate Farallón Negro district (Fig. 1) is the Agua Rica Cu–Mo–Au deposit (Perelló et al. 1998; Rojas et al. 1998; Landtwing et al. 2002). Here high-sulfidation alteration overprints more typical porphyry-style mineralization (Landtwing et al. 2002).

Miocene stratigraphy

The Late Miocene Farallón Negro Volcanics rest conformably on the Middle Miocene El Morterito Formation, which consists almost entirely of basement-derived sandstone, red and red-brown siltstone, and minor conglomerate. Across the Farallón Negro district, the formation comprises thick, dominantly planar to cross-bedded, micaceous sandstone and red siltstone. In places, a thin transitional sequence (£ 10 m thick) is recognized between the El Morterito Formation and Farallón Negro Volcanics; it is characterized by pebbly sandstone, conglomerate, and sedimentary breccia of mixed (basement and proximal volcanic) provenance.

The Farallón Negro Volcanics are subdivided into eight principal lithofacies that are grouped into lower mafic to intermediate and an upper intermediate to silicic volcanic and volcaniclastic facies associations (Table 1, Fig. 3). Both facies associations are dominated by coarse-grained sedimentary lithofacies reflecting erosion of proximal volcanic material. The associations record an up-sequence evolution of multi-vent volcanism that differed in eruptive style (from effusive to mixed effusive and explosive) and composition (from mafic to intermediate-silicic).

The base of the Farallón Negro Volcanics is defined by a relatively abrupt change to coarse-grained, angular volcanic provenance and an associated absence of basement-derived material. Distinctive, coarse-grained clinopyroxene-phyric basaltic volcanic rocks occurring primarily as multiple, syn-sedimentary intrusions with peperitic margins, as well as dykes and minor lavas, occur at the contact between the El Morterito Formation and the Farallón Negro Volcanics. The lower mafic volcanic and volcaniclastic lithofacies association is dominated by bedded (1–15 m thick), matrix- to clast-supported, polymictic mafic volcanic (clinopyroxene-, plagioclase-phyric), pebble- to boulder-grade sedimentary breccias. Bedding is generally sheet-like, although several beds have erosive lower contacts. Many sedimentary breccia beds show long-axis imbrication, bedding alignment, coarse-tail grading, and grain stratification, suggesting deposition from hyperconcentrated flood flows. The thicker, more massive and poorly sorted sedimentary breccias are interpreted to have been emplaced from debris flows and hyperconcentrated flood flows. Thin intervals of stratified to massive lithic sandstone commonly separate the breccia beds.

The upper intermediate to silicic volcanic and volcaniclastic lithofacies association is dominated by exogenous to endogenous lava domes and autobreccias. The lava domes are internally complex, exhibiting rapid lateral and vertical transitions from coherent to brecciated facies, and appear to be buried by thick matrix-supported poorly vesiculated juvenile clast-dominated breccias interpreted to be block and ash flow deposits. Intercalated with the lava domes are matrix- to clast-supported, poorly sorted juvenile clast-dominated breccias of intermediate to silicic composition (predominantly hornblende-, biotite-, plagioclase-phyric), interspersed with thin, discontinuous intervals of red-brown sandstone and siltstone. Peperitic intrusions are also distinctive throughout this upper facies association. Several rhyolitic phreatomagmatic base surge and fall-out deposits, along with some ignimbrites, form distinctive lithofacies in the upper association. At one locality, the phreatomagmatic deposits are partly eroded by an overlying thick, massive, matrix-supported sedimentary conglomerate that contains boulders of crystalline basement. The massive to slightly stratified, disorganized and poorly sorted character of the conglomerates suggests emplacement from debris flows (Hwang et al. 1995); however, the flows were also erosive, with some beds exhibiting erosive bases (i.e., low-angle scours), incorporation of rip-up clasts, and substrate erosion.

Characteristics of volcanic rocks and subvolcanic intrusions of the Farallón Negro Volcanics

Temporally, the volcanic and subvolcanic intrusions of the Farallón Negro district show a change from mafic to bimodal intermediate-silicic compositions (Table 2; Fig. 4). The earliest primary volcanic units are clinopyroxene-phyric basaltic andesite, characterized by conspicuous euhedral clinopyroxene (2–5 mm) macrocrysts, and rarer plagioclase (1–2 mm; An_{37}–An_{48}), set in a fine-grained, aphanitic groundmass of plagioclase with trace magnetite and titanite. These are subvolcanic intrusions and subaerial lavas (<25 m thick) that occur to the southwest of the Bajo de la Alumbrera mine and along the western foothills of Sierra Durazno (the mountain chain to the east of Alumbrera). Blocky peperite textures occur along the contacts of several broadly concordant intrusions. Where subaerial lavas occur, the sedimentary rocks underlying the basal contacts are indurated and baked. Close to the Bajo de la Alumbrera mine there are thick (<75 m) hornblende (±clinopyroxene)-phyric andesite dykes and sills. Hornblende and clinopyroxene phenocrysts (<3 mm) are set in a fine-grained plagioclase (An_{45}–An_{58}) groundmass with magnetite and titanite. In general, these intrusions are discordant to

Table 1 Summary of the principal lithofacies and lithofacies associations in the Farallón Negro Volcanics

Facies	Characteristics	Interpretation
Upper intermediate to silicic volcanic and volcaniclastic lithofacies association		
Facies 8: Andesite to dacite block-and-ash flow deposits	Near monomictic breccia dominated by dense, angular juvenile lava (either andesite or dacite) supported in a finer-grained, crystal-rich lapilli and ash matrix. Clasts exhibit jigsaw-fit textures of blocky and wedge-shaped clasts supported by minor amounts of comminuted coherent lava and crystal-rich volcanic lapilli and ash	Gravitational or explosion-triggered collapse, or vertical or laterally directed, explosive eruption columns accompanying lava dome extrusion. Block-and-ash flows
Facies 7: Andesite to dacite lava	Evenly porphyritic; columnar jointing; massive or flow banded; blobby glass matrix. Outcrops are either sheet-like or form dome-like bodies. Associated lava breccias	Sills and dykes surrounding endogenous (and possibly exogenous) lava domes
Facies 6: Andesite to dacite peperite	Evenly porphyritic; columnar jointing; massive or flow banded; blobby glass matrix. Monomictic; angular to subangular blocky, ragged and equi-dimensional clasts (5–80 cm; outsized clasts are up to 3 m) of poorly vesiculated hornblende-, biotite-, plagioclase-phyric andesite to dacite; clast to matrix supported; spalled clasts and jig-saw fit common; non erosive irregular base; crystal rich sandstone matrix; wispy siltstone clasts in base	Syn-sedimentary sills and dykes with in situ quench fragmentation. In situ quench fragmentation formed from magma intruded into wet, unconsolidated sediment
Facies 5: Basement clast-bearing boulder-grade conglomerate	Coarse quartz-lithic sandstone and pebbly sandstone, and pebble to boulder-sized conglomerate. Conglomerates are massive, poorly sorted, and polymictic with abundant rounded to subangular clasts of crystalline basement rocks (e.g., coarse-grained feldspar granite)	Alluvial fan and unconfined fluviatile deposits derived in part from exposed crystalline basement
Facies 4: Bedded sedimentary conglomerates and red siltstones	Polymictic; well rounded to angular clasts (1–50 cm); massive to normally graded; coarse feldspathic and lithic sandstone matrix; erosive base; interbedded laminar siltstone and pumiceous siltstone	Fluviatile and ephemeral lacustrine deposits; suspension sedimentation
Facies 3: Bedded crystal-rich ash and lapilli tuff	Planar, well bedded pumice and crystal rich ash and lapilli sandstone interbedded with quartz lithic sandstone; accretionary lapilli mudstone; clast and matrix support granular conglomerate; well rounded basement metamorphic clasts	Rhyolitic phreatomagmatic base surge and fallout deposits
Lower mafic to intermediate volcanic and volcaniclastic lithofacies association		
Facies 2: Basaltic to basaltic andesite volcanic-derived sedimentary breccias	Polymictic matrix supported breccia dominated by angular to subrounded mafic (clinopyroxene-, plagioclase- phyric basalt, basaltic andesite, andesite and dacitic clasts; 5–50 cm) set in fine- to coarse-grained quartz lithic sandstone; thick bedded (1 fi 10 m), reverse or normal grading; sharp to erosive base. Breccia exhibit long axis imbrication, bedding alignment, coarse-tail grading and grain size stratification or laying	Debris and hyper-concentrated flood flows
Facies 1: Coherent basaltic andesite and associated non-stratified basaltic andesite breccia	Evenly porphyritic, coarse grained pyroxene and plagioclase–pyroxene phyric basaltic andesite with angular blocks (<60 cm) of same composition found throughout; amygdaloidal; wispy siltstone clasts and siltstone dykes are common along the basal contacts. Monomictic angular and blocky breccia with clasts and matrix exhibiting uniform composition of coarse grained pyroxene phyric basaltic andesite	Syn-sedimentary sills and dykes with in situ quench fragmentation. Minor lava flows. In situ quench fragmentation formed from magma intruded into wet, unconsolidated sediment

Table 2 Characteristics of volcanic and subvolcanic units of the Farallón Negro Volcanics. Bt biotite; Cpx clinopyroxene; Kflds K-feldspar; Plag plagioclase; Qtz quartz; N.D. not defined

Intrusive phase	Phenocrysts[a]	Comments
Pre-mineralization		
Basaltic andesite — Lower Basaltic Andesite	Plag (2–4 mm, 5–10%); Cpx (<5 mm; <15%)	Peperitic sills and dykes
Andesite	Plag (2–3 mm, <5%); Cpx (<5 mm, <5%)	Sills and dykes
Andesite — Durazno Andesite	Hbl (2–7 mm; <5%); Plag (<2 mm, <20%), Qtz (<1 mm; <5 mm)	Stocks, dykes and peperitic sills
Syn-mineralization (barren)		
Andesite — La Chilica Andesite	Hbl (<2 mm, <5%), Cpx (<2 mm, <5%), Plag (<1 mm, <10%)	Sills and dykes
Dacite — Dionisio Dacite	Bt (<5 mm, <5%), Hbl (<2 mm, <2%), Plag (1–5 mm, <30%), Qtz (<5 mm, <10%)	?Stocks, diatremes
Trachyandesite — Alto de la Blenda Andesite	Hbl (<2 mm, <5%), Bt (<5 mm, <5%), Plag (1–5 mm, <30%), Kflds (<1 mm, <30%)	Stocks, sills, and dykes
Trachyandesite — Aguila Dykes	Hbl (<2 mm, <2%), Cpx (<2 mm, <5%), Plag (<2 mm, <10%)	Dykes
Syn-mineralization (Cu–Au)		
Dacite — Alumbrera Dacite	Hbl (2–3 mm, <2%), Bt (<5 mm, <5%), Plag (1–5 mm, <30%), Qtz (<5 mm, <15%)	Stocks and dykes
Dacite — Agua Tapada Dacite	Hbl (2–3 mm, <2%), Bt (<5 mm, <5%), Plag (1–5 mm, <30%), Qtz (<5 mm, <10%)	Stocks, dykes
Post-mineralization (Cu–Au)		
Basaltic andesite	Plag (<3 mm, <15%)	Dykes, sills, and plugs
Rhyodacite — Macho Muerto Rhyodacite	Hbl (2–3mm, <5%), Bt (<5mm, <2%), Plag (<10 mm, <15%) Kflds (<40 mm, <2%)	Sills and dykes

[a]Percentages are averages of visual estimates of vol% in thin sections and cut slabs; grain sizes refer to long dimensions

sedimentary bedding. However, two concordant lavas occur in the southern wall of the Bajo de la Alumbrera mine, where vesiculated coherent basaltic andesite is interlayered with clast-supported breccia zones. Herein, we group these basaltic andesite rocks as part of the Durazno Andesite (after Llambías 1972), which includes the Lower Basaltic Andesite (after Proffett 1997).

Hornblende-phyric andesitic sills, stocks, dykes intrude the Durazno Andesite. The rocks are characterized by stubby macrocrysts of hornblende (<7 mm), smaller biotite laths (<2 mm), and plagioclase phenocrysts (<2 mm, An_{65}–An_{70}) set in a fine-grained plagioclase (An_{38}) dominated groundmass with rare sanidine, quartz, magnetite, and clinopyroxene phenocrysts. These rocks are assigned to the La Chilica Andesite after Llambías (1972).

Intruding the La Chilica Andesite and the Durazno Andesite are plagioclase–biotite-phyric dacite stocks and dykes. Referred to as the Alumbrera Dacite (a new subdivision), these dacites are dominated by phenocrysts of plagioclase (<5 mm, An_{65}–An_{78}), biotite (<3 mm) and rare hornblende and quartz set in a fine-grained feldspathic groundmass. Quartz phenocrysts can be distinctly pink with a rounded form. The Alumbrera Dacite is recognized in this study as a petrologically (and as will be shown, a temporally) distinct group that has been historically included within the mineralized Aqua Tapada Dacite porphyries (as defined by Llambías 1972). Subsequent porphyry intrusions have larger (1–8 mm) and more abundant hexagonal platy books of biotite (Proffett 1997). Within these particular porphyry phases there are basaltic inclusions. The presence of these inclusions may, in part, be evidence of mingling and/or incomplete mixing (Sasso 1997; Ulrich and Heinrich 2001; Harris 2002). The Agua Tapada Dacite occurs at all the mineralized porphyry occurrences and deposits in the Farallón Negro district.

Proffett (personal communication 2001) has proposed that the Aqua Tapada Dacite porphyries at Bajo de la Alumbrera are, in part, co-temporal with biotite (hornblende)–plagioclase phyric dacite lava domes that occur in the NW of the volcanic complex, based on distinct petrologic similarities to the mineralized porphyries. Referred to as the Dionisio Dacite by Proffett (personal communication 2001), they are characterized by phenocrysts of hornblende (<2 mm), biotite (<5 mm), and quartz eyes (<5 mm) surrounded by finer, euhedral plagioclase (0.2–1 mm, An_{62}–An_{72}) groundmass.

In the south of the district, there are two rhyodacitic diatremes. El Espanto, southwest of Bajo de la Alumbrera (Proffett 1997, personal communication 2001), is mineralized with chalcopyrite–quartz veined porphyry fragments, whereas the unnamed diatreme to the south of Bajo las Pampitas is barren (Fig. 2). Both diatremes are characterized by medium-grained, polymictic rhyolitic and andesitic breccia rims and more massive and fine-grained, well-bedded monomictic breccia in the center. The breccias have weak pervasive sericite

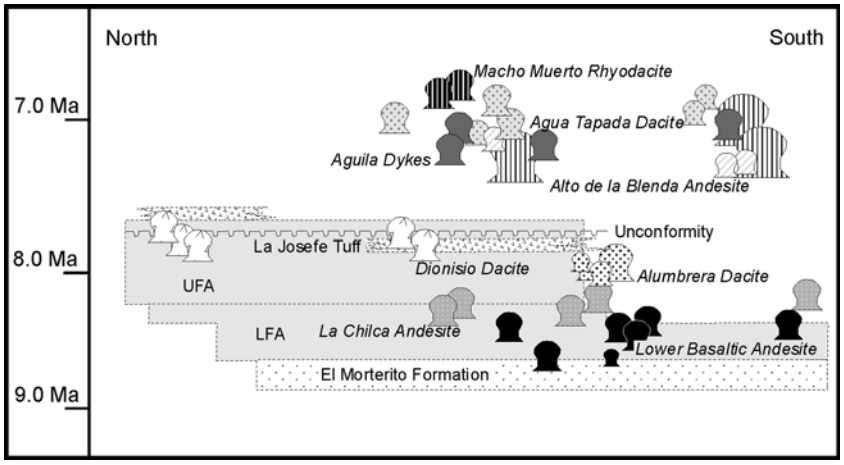

Fig. 4 Schematic relationship (time and space) diagram of the subvolcanic intrusions relative to the volcanic stratigraphy. The U–Pb zircon geochronology constrain the temporal relationships. Note that the lava domes complexes (and subvolcanic intrusions) of the Dionisio Dacite (Proffett 1997) are co-temporal with the mineralized and altered porphyritic intrusions of the Alumbrera Dacite (this study). The LFA and UFA refers to the lower and upper facies associations, respectively (see Fig. 3)

(±tourmaline) alteration. Irregular, weakly chloritic-altered plagioclase ± biotite phyric dacite dykes cross-cut the diatremes.

The Alto de la Blenda Andesite stock occurs near the center of the Farallón Negro district (Fig. 2). It is equigranular and fine-grained (<1.5 mm), composed principally of plagioclase, clinopyroxene, and hornblende, with rare magnetite, quartz, sanidine, and biotite. Smaller equivalent intrusions, commonly with much coarser phenocrysts of hornblende (<3 mm), are found north of this larger stock and occur as stocks, dykes, and sills. At Bajo las Pampitas, the porphyry Cu–Au occurrence to the NW of Bajo de la Alumbrera, the Alto de la Blenda Andesite, is intruded by mineralized biotite-phyric dacites. However, the relative timing between the Alumbrera Dacite and the Alto de la Blenda Andesite is uncertain. Additionally, fine-grained hornblende phyric basaltic trachyandesite of the Aguila dykes cut the Alto de la Blenda Andesite. Their timing relative to the dacites at Bajo las Pampitas is also unknown (Fig. 2).

The youngest intrusion in the district is the Macho Muerto Rhyodacite, which occurs as discontinuous sills and dykes in the NW of the Farallón Negro district. It is sanidine–biotite-phyric with sanidine occurring as megacrysts (<10 cm), surrounded by fine-grained macrocrysts of biotite (<1 mm), hornblende, plagioclase, and quartz. Clinopyroxene occurs as diffuse and embayed phenocrysts.

Intrusive geology of the Bajo de la Alumbrera porphyry Cu–Au deposit

Numerous published and company reports document the intrusions, hydrothermal alteration, and deposit paragenesis of Bajo de la Alumbrera (e.g., González 1975; Godeas and Segal de Svetliza 1980; Stults 1985; Dawson 1994; Guilbert 1995; Méndez 1997). The most comprehensive studies undertaken to date are the unpublished maps and reports produced by J.M. Proffett (1995, 1997) that outline the apparent cross-cutting relationship of the porphyritic intrusions and hydrothermal alteration in the deposit. Ulrich and Heinrich (2001) added to Proffett's work in summarizing the geology of Bajo de la Alumbrera (Fig. 5), and used this for detailed geochemical studies of the hydrothermal alteration and mineralization.

At Bajo de la Alumbrera, alteration is spatially and temporally related to the emplacement of six plagioclase–biotite (hornblende)-phyric dacite porphyries (J.M. Proffett, personal communication 2001). Figure 5 shows the distribution of the porphyry phases. Alteration within the Bajo de la Alumbrera deposit is zoned from a central quartz–magnetite and potassic (biotite–K-feldspar ± quartz) altered core, outwards through phyllic (quartz–muscovite–illite ± pyrite), intermediate argillic (chlorite–illite), and propylitic (chlorite–illite–epidote–calcite) assemblages. Similar alteration zones occur at Bajo el Durazno and Bajo las Pampitas; however, the contained mineralization is subeconomic. Mineralization at the Bajo Agua Tapada porphyry-related occurrence is centered on pervasive phyllic (muscovite–illite) and argillic (kaolinite) alteration.

The Los Amarillos Porphyry is one of the earliest porphyries at Bajo de la Alumbrera (Proffett 1997). Although the strong pervasive alteration has destroyed primary igneous textures, the Los Amarillos Porphyry appears to be biotite–plagioclase–phyric, commonly with distinct rounded quartz phenocrysts and angular quartz vein fragments. Proffett (1997) was uncertain about its relationship to later porphyries (e.g., Early P3), and proposed that it may be an igneous breccia along the Early P3 contact.

Previously, the main stage of Cu–Au mineralization at Bajo de la Alumbrera has been attributed to the emplacement of the P2 (or Colorado Norte) Porphyry phase (Proffett 1997). Unlike most porphyry intrusions in the Bajo de la Alumbrera deposit, P2 lacks quartz vein fragments and has not been seen to truncate vein and fracture-controlled mineralization (Proffett 1997). Strong pervasive alteration obscures primary igneous textures, but relict phenocrysts show it was a plagioclase-phyric dacite with minor biotite and hornblende

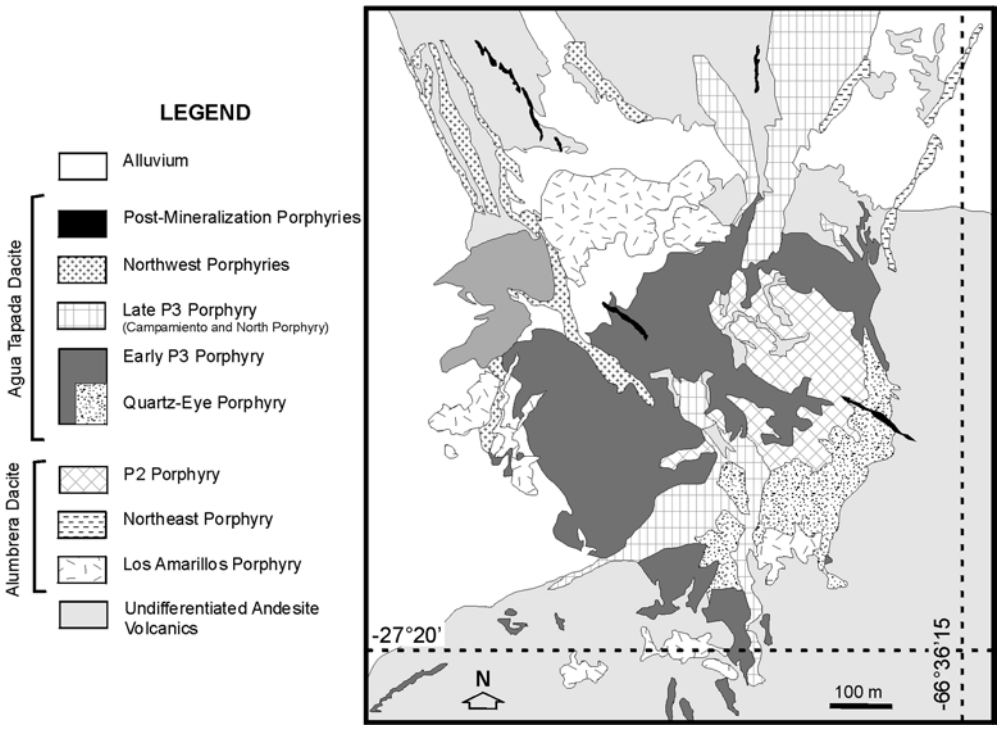

Fig. 5 Generalized geologic map of the porphyritic intrusions at Bajo de la Alumbrera (complied from J.M Proffett's 1995 mapping and published by Ulrich and Heinrich 2001). The figure also includes the new subdivision of the intrusions based on the new U–Pb zircon geochronology

phenocrysts. Intruding P2, the Early P3 Porphyry is a biotite- and plagioclase-phyric dacite that contains fragments of andesite wall rock and mineralized quartz veins. Subtle variations in the content of different macrocrysts show that there is are several phases of the Early P3 Porphyry (Proffett 1997). The Quartz Eye Porphyry is one containing more abundant quartz eyes than Early P3. This study groups these similar porphyries as Early P3. The Northeast Porphyry occurs on the edge of the central Alumbrera porphyries. It is weakly mineralized, but contains much fewer quartz phenocrysts than most porphyries. As there are no clear crosscutting relationships, its timing is unknown (Proffett, personal communication 2001). The Northeast Porphyry is petrographically similar to the Early P3 porphyries, and is inferred to be related to them (Ulrich and Heinrich 2001).

The Late P3 porphyries (including the Campamiento and North porphyries) are a group of hornblende- and plagioclase-phyric dacite porphyries that contain distinctive euhedral ''book'' biotites (Proffett 1995, 1997; Ulrich and Heinrich 2001). At depth, some of these porphyries are more equigranular, more like a monzonite. Although they are weakly altered by potassic and propylitic assemblages and are weakly quartz veined, these porphyries are believed to post-date main-stage mineralization (Proffett, personal communication 2001). Other porphyry phases that are petrographically very similar to the Late P3 porphyries, but contain more abundant and larger resorbed quartz phenocrysts, include the Northwest and Post-Mineralization dykes (as defined by Proffett 1997, and summarized in Ulrich and Heinrich 2001).

Previous geochronology studies

Early workers on the Farallón Negro district inferred a Neogene age for the volcanic rocks, based on stratigraphic relationships (e.g., González Bonorino 1950): this was subsequently confirmed by K–Ar age determinations published by Caelles et al. (1971). Sasso and Clark (1998) reported the most extensive geochronology for the Farallón Negro district. This work summarized the total fusion and step-heating analyses undertaken by Sasso (1997). These laser probe $^{40}Ar/^{39}Ar$ ages confirmed the K–Ar age data of Caelles et al. (1971) and Clark et al. (1976), indicating that Late Miocene volcanism in the district coincided with that of northern Chile, and that the main arc broadened rather than migrated during the Middle Miocene (Sasso and Clark 1998). They also reported that the onset of volcanism began at 12.56±0.36 Ma (2σ uncertainty, hornblende) and persisted until 5.16±0.05 Ma (biotite), with the peak of intrusive activity found between 8.6 and 5.2 Ma (Sasso and Clark 1998).

Dacitic intrusions at the Bajo de la Alumbrera porphyry Cu–Au deposit have ages that range from 7.10±0.13 to 6.83±0.07 Ma (biotite; Sasso and Clark 1998). These samples were collected from a zone of intense potassic alteration (K-feldspar–biotite) so it is possible that the biotite (including phenocrystic biotite) has been reset by the hydrothermal alteration. The same age has been reported for the phyllic (quartz–sericite–pyrite) alteration at Bajo de la Alumbrera and the alteration of the Farallón Negro-Alto de la Blenda Au–Ag veins that occur about 10 km to the northwest of

Bajo de la Alumbrera (6.55±0.14 Ma, whole-rock; Sasso and Clark 1998).

U–Th–Pb analytical method

U–Th–Pb isotopic compositions of zircons were analyzed at the Australian National University, Canberra, using Excimer laser ablation inductively coupled plasma mass spectrometry (ELA-ICP-MS). The zircons were separated from 1 kg samples by conventional magnetic and heavy liquid separation techniques. The extracted zircons were mounted in epoxy resin and polished. Cathodoluminescence and optical photomicrographs were used to select least fractured and inclusion-free zircons for analysis.

Dating by ELA-ICP-MS followed a procedure described in Ballard et al. (2001). Samples were ablated with a pulsed 193 μm ArF LambdaPhysik LPX 1201 UV Excimer laser with constant 100 mJ energy, a repetition rate of 5 Hz and a pit diameter of 29 μm. A mixed Ar–He (with minor H_2) carrier gas transported the ablated material from the sample cell into a flow homogenizer to an Agilent 7500 ICP-MS. Counts for ^{39}Si, ^{96}Zr, ^{31}P, ^{206}Pb, ^{207}Pb, ^{208}Pb, ^{232}Th, and ^{238}U were collected in time-resolved mode. Because of a high ^{204}Hg blank, believed to reside in the carrier gas, ^{204}Pb was not measured. Other isotopes analyzed during age determinations were ^{139}La, ^{140}Ce, ^{144}Sm, ^{146}Nd, ^{175}Lu, and ^{178}Hf.

The integration time for the three Pb isotopes was 50 ms, 25 ms for U and Th, and for all other isotopes it was 5 ms with a total mass sweep time of 0.4 s. Background was measured for 20 s with the laser turned off, and the sample measured for a further 40 s with the laser turned on, giving ~120 mass scans for a penetration depth of ~30 μm.

After triggering the laser, it took approximately 10 mass scans to reach a steady signal, so the initial data were excluded from data reduction. Depth-dependent inter-element fractionation of Pb, Th, and U (e.g., Hirata and Nesbitt 1995; Horn et al. 2000) was corrected by reference to multiple measurements of standard zircon TEMORA and NIST612 silicate glass (Pearce et al. 1997; Black et al. 2000). Measured ^{207}Pb/^{206}Pb, ^{206}Pb/^{238}U, and ^{208}Pb/ ^{232}Th ratios in TEMORA, and ^{232}Th/^{238}U in NIST612, were averaged over the analytical day and used to calculate correction factors for each mass sweep down the ablated hole. These factors were applied to each time slice to correct for instrumental mass bias and depth-dependent elemental and isotopic fractionation. Common Pb (the difference between the measured and expected ^{208}Pb/^{206}Pb, given a preliminary ^{206}Pb/^{238}U age and Th/U) was then subtracted (Compston et al. 1984), assuming a common Pb composition from the age-dependent Pb model of Cumming and Richards (1975). Common ^{206}Pb is generally less than 1% of total ^{206}Pb. Given the age of the rocks analyzed here, model common Pb compositions do not vary greatly, and, at this level of common Pb, what model is selected is irrelevant in terms of the calculated age (affecting a maximum change of 0.2%). In most cases, the resulting ratios were concordant within analytical uncertainty where we use agreement of ^{206}Pb/^{238}U and ^{207}Pb/^{235}U ages as a measure of concordancy. Reported ages are the weighted mean ^{208}Pb-based common Pb-corrected ^{206}Pb/^{238}U ages (but see additional Th-disequilibrium correction below). Quoted uncertainties on individual samples are two times the standard uncertainty of corrected ^{206}Pb/^{238}U age for the selected portion of the population. For rocks analyzed during the same analytical session, these uncertainties can be quoted when comparing those populations.

If single analyses from different days or populations reduced with respect to different standard sets are to be rigorously compared, then the uncertainty in the Pb/U of the standard must be incorporated. As mentioned below, over an analytical session this may display a total variation of 2 to 3%. When this uncertainty from the standard is added to the standard error in an individual analysis, the overall uncertainties quoted here increase by 10 to 15% on an individual analysis, and significantly reduces MSWD for a population (but see the day-to-day consistency of measured mean ages below).

Data exclusion is on the basis of four criteria. Firstly, spectra are examined for inclusions. Analyses with anomalously high La (i.e., >3 ppm) and/or high P values (i.e., >500 ppm) suggest that an apatite inclusion might have been intersected. Because apatite commonly has high common lead concentrations, the analysis was discarded (see Watson et al. 1997). Portions of analysis deemed inclusion free and having over 15 time slices are selected. Once the analyses for a sample are complied, then an additional three filters are applied: (1) If the observed/expected uncertainties on ^{208}Pb/^{238}U exceeds 2, the grain is excluded as a ratio greater than this could indicate a mixture of age domains (but note that this is relaxed to 3 in the cases of inherited grains >200 Ma); (2) if concordancy as reflected by the ratio of 208-based common-Pb-corrected ages (^{206}Pb/^{238}Uage / ^{207}Pb/^{235}U age) is not within the range 0.9 to 1.1, the grain is interpreted as discordant and, therefore, rejected (note that this criterion was relaxed between 0.8 and 1.2 for one sample, ACH00245, which has a high common Pb component); (3) based on the shape of the probability plots (inset Fig. 6), subtle inheritance or Pb loss was

c

Fig. 6 Concordia plots and probability plots of ELA-ICP-MS U–Pb results used in calculating the ^{206}Pb/^{238}U zircon ages of individual samples from the Farallon Negro district. Sample numbers listed in the top right hand corner corresponds to those listed in Table 3. On the concordia portion: the uncorrected data are circles, where the filled equals the selected data used for the final age calculation. Those samples plotting off the diagram indicated by arrows. The open circles are the omitted data. Crosses are data both ^{208}Pb and ^{230}Th corrected with 2σ uncertainties including uncertainties in standards. On the smaller probability diagram all ^{208}Pb and ^{230}Th corrected data are plotted as squares, with the data omitted on this probability plot basis shown as the open symbols. Note common Pb is significant in many samples, but the ^{208}Pb correction works well

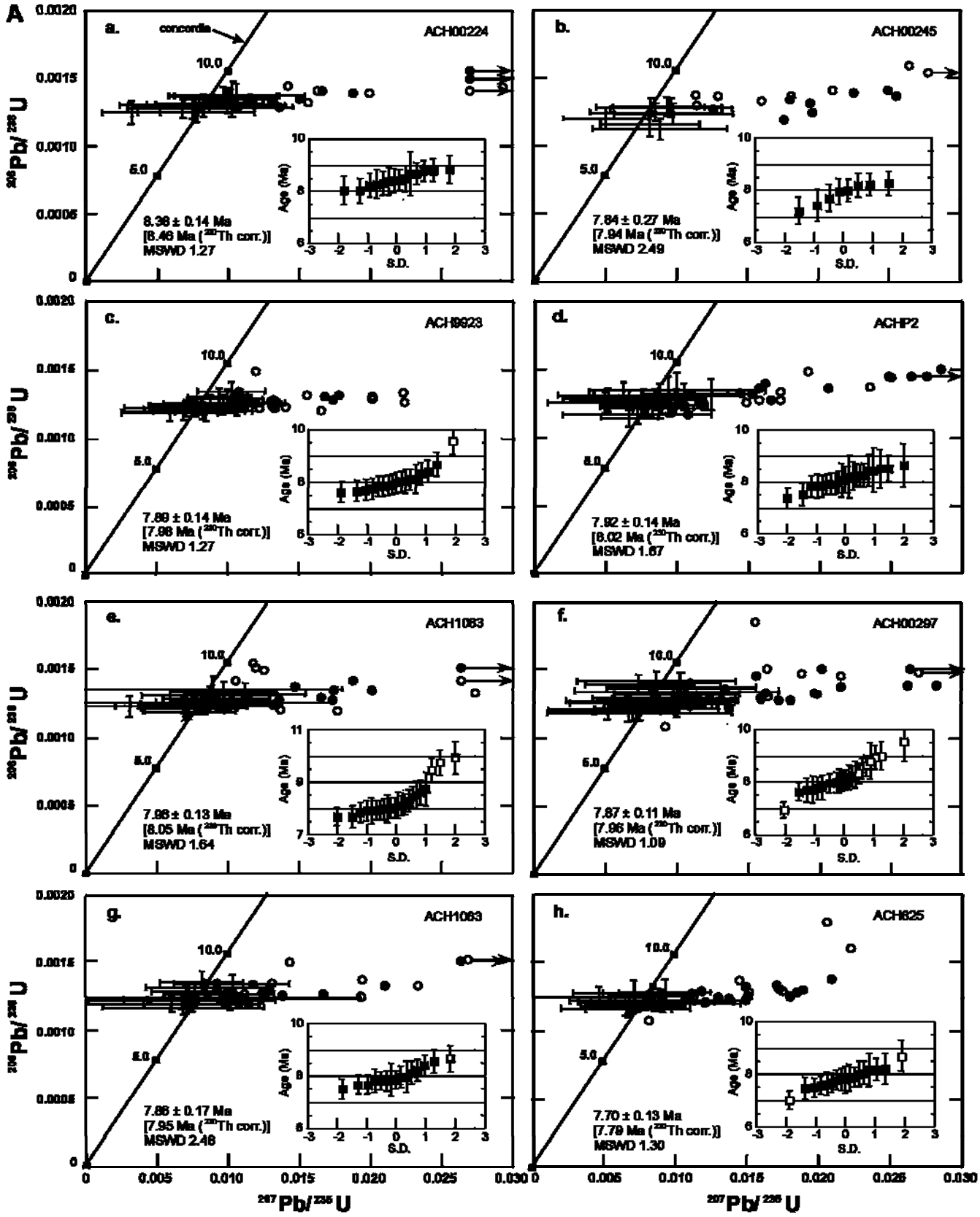
A
a.
concordia
ACH00224
8.36 ± 0.14 Ma
[8.46 Ma (230Th corr.)]
MSWD 1.27
b.
ACH00245
7.84 ± 0.27 Ma
[7.94 Ma (230Th corr.)]
MSWD 2.49
c.
ACH9923
7.89 ± 0.14 Ma
[7.98 Ma (230Th corr.)]
MSWD 1.27
d.
ACHP2
7.92 ± 0.14 Ma
[8.02 Ma (230Th corr.)]
MSWD 1.67
e.
ACH1083
7.96 ± 0.13 Ma
[8.05 Ma (230Th corr.)]
MSWD 1.64
f.
ACH00297
7.87 ± 0.11 Ma
[7.96 Ma (230Th corr.)]
MSWD 1.09
g.
ACH1083
7.86 ± 0.17 Ma
[7.95 Ma (230Th corr.)]
MSWD 2.46
h.
ACH625
7.70 ± 0.13 Ma
[7.79 Ma (230Th corr.)]
MSWD 1.30
Age (Ma)
S.D.
206Pb/238U
207Pb/235U

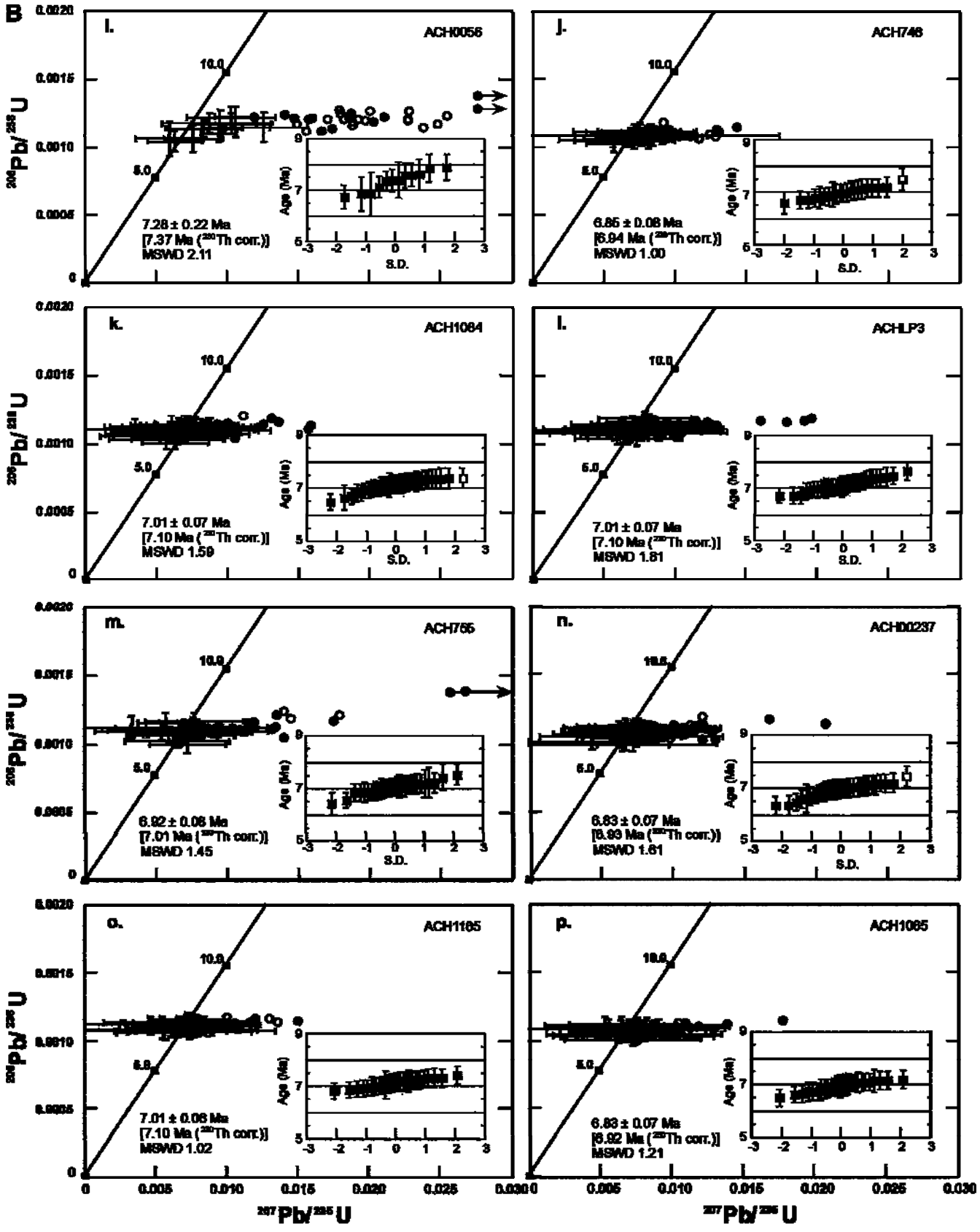
B
I.
ACH0056
7.28 ± 0.22 Ma
[7.37 Ma (230Th corr.)]
MSWD 2.11
J.
ACH746
6.85 ± 0.08 Ma
[6.94 Ma (230Th corr.)]
MSWD 1.00
k.
ACH1084
7.01 ± 0.07 Ma
[7.10 Ma (230Th corr.)]
MSWD 1.59
l.
ACHLP3
7.01 ± 0.07 Ma
[7.10 Ma (230Th corr.)]
MSWD 1.61
m.
ACH765
6.92 ± 0.08 Ma
[7.01 Ma (230Th corr.)]
MSWD 1.45
n.
ACH00237
6.83 ± 0.07 Ma
[6.93 Ma (230Th corr.)]
MSWD 1.61
o.
ACH1165
7.01 ± 0.08 Ma
[7.10 Ma (230Th corr.)]
MSWD 1.02
p.
ACH1065
6.83 ± 0.07 Ma
[6.92 Ma (230Th corr.)]
MSWD 1.21
Age (Ma)
S.D.
206Pb/238U
207Pb/235U

Fig. 6 (Contd.)

identified and rejected. Generally, this reduces the population MSWD to <2.0.

Zircons from the Farallón Negro Volcanic Complex form two morphologic populations: the first are pink prismatic euhedral crystals ranging from <50 to 350 μm long; the second population consists of clear rounded stubby euhedral crystals, characteristically <50 μm long. Most zircons contain minor apatite inclusions and rounded elongate melt inclusions. Cathodoluminescence images of polished grains show thick mantles of fine oscillatory zoning over centers that exhibit broader more diffuse zonation patterns (Fig. 7). The truncation of growth bands indicative of resorption is rare in the zircons analyzed and no morphological characteristics can be used to discriminate inherited cores.

Analytical precision and accuracy

The accuracy of the ELA-ICP-MS technique has been proven by repeat analysis of porphyritic intrusions from the Chuquicamata mine, Chile, combined with comparative SHRIMP analyses (Ballard et al. 2001). Like SHRIMP, the ELA-ICP-MS zircon U–Pb technique reported here is a relative geochronologic method, in which the age of the mineral is calculated relative to the age of a mineral standard (e.g., Fish Canyon Tuff reference standard, Lanphere and Baadsgaard 2001). Thus, the ultimate accuracy of the method is governed by standard homogeneity, how well the age of zircon standard is known, and how well it can be repeatedly measured. SHRIMP U–Pb data ultimately rely on standards that have had their homogeneity and isotopic ratios established by traditional TIMS U–Pb analysis (Compston et al. 1984). Here we use the TEMORA standard (416.8±0.2 Ma; Black et al. personal communication 2002), which consists of zircons from a gabbroic diorite in central New South Wales, Australia (Black et al. 2000). If, for a given 10 h analytical day, we reduce TEMORA zircons as unknowns against the average of the same data set used for reduction of unknown zircons, we get $^{206}Pb/^{238}U$ age scatter of about 3% so that an individual analysis cannot be more precise than this. We attribute this scatter to inhomogeneity in the standard and instrument drift.

The problem of standard heterogeneity is not unique to the ELA-ICP-MS technique (Lanphere and Baadsgaard 2001). To test whether the ICP-MS method was suitable for dating rocks as young as those in the Farallón Negro district, a sample of the ~12 Ma Naxos granodiorite from the Cyclades, Greece, was analyzed (NX9301; Keay 1998). The age of this rock has already been determined by several techniques (as summarized by Keay 1998). These include a whole-rock Rb–Sr age of 11.7±0.8 Ma, as well as K–Ar and Rb–Sr (biotite) ages of approximately 11 Ma for the granodiorite (Durr et al. 1978). Wijbrans and McDougall (1988) report an $^{40}Ar/^{39}Ar$ plateau age of 12.2 Ma (hornblende) and interpreted this to be the cooling age of the granodiorite. More recent K–Ar analysis of biotite yielded an age of 12.3±0.4 Ma (Pe-Piper et al. 1997). The age of the Naxos granodiorite has also been determined by SHRIMP U–Pb zircon analyses, returning a $^{206}Pb/^{238}U$ age of 12.2±0.1 Ma (n=22) and titanite analyses with an age of 11.8±0.9 Ma (n=38; Keay 1998). Our new ELA-ICP-MS U–Pb zircon age for the Naxos granodiorite is 12.31±0.07 Ma with an MSWD of 0.51 for 25 of 33 grains analyzed. Six grains were clearly inherited and were not used in the age determination. As were zircons containing apatite inclusions. This technique comparison indicates that, in dating Miocene rocks, ELA-ICP-MS will produce an age within uncertainty of the SHRIMP age, and this is irrespective of differences in the standards used between the dating techniques, i.e., SL13 versus TEMORA. Furthermore, these ages are comparable to those determined by the K–Ar and $^{40}Ar/^{39}Ar$ methods.

The reproducibility of the ELA-ICP-MS technique was monitored by repeat analysis of an in-house

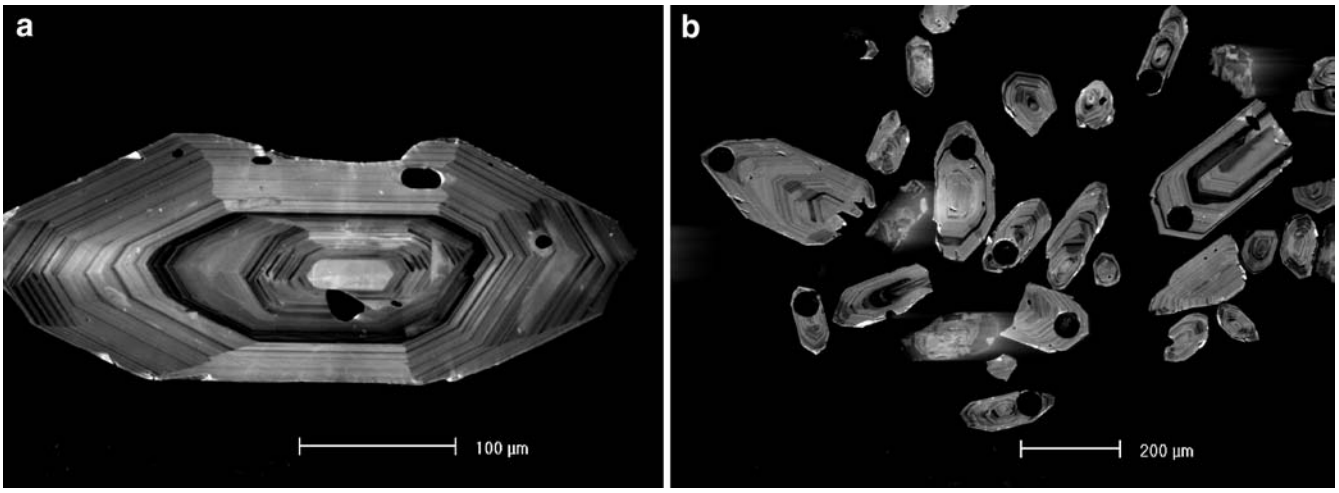

Fig. 7 Cathodoluminescence images of zircons from the Farallón Negro Volcanic Complex: a Shows the fine igneous growth bands over a distinct core. Apatite inclusions occur along these fine outer growth bands. b Igneous zircons after laser ablation of the zircon tips

standard, the Los Picos porphyry from the Fortuna Complex, Chile (ANU # 98-521; Ballard 2001). Although the zircons from the Los Picos porphyry contained apatite inclusions, it was found that the four calculated ages each from an analytical day of about 30 analyses all lie within analytical uncertainty of each other (i.e., 42.31±0.23; 41.85±0.25; 42.49±0.30; 42.46± 0.42 Ma). These ages are coincident with that previously established for this sample using the ICP-MS (42.2± 0.2 Ma; Ballard 2001). Reproducibility of the ages determined for the Farallón Negro Volcanics was tested by repeat analysis of a single porphyritic intrusion at Bajo de la Alumbrera. It was found that two igneous ages, calculated on two analytical days, were within analytical uncertainty (i.e., 7.06±0.13; 7.03±0.04 Ma) — the discrepancy between these ages could be a function of different population sizes used to calculate the age. The ELA-ICP-MS produces ages that are comparable to those obtained by other widely used methods (e.g., $^{40}Ar/^{39}Ar$) and that the results are reproducible for Miocene rocks.

U–Pb geochronologic results

U–Th–Pb systematics

Data from 18 samples analyzed by ELA-ICP-MS U–Pb geochronology are summarized in Table 3. The complete data table is supplied in the Supplementary Electronic Marerial. Between 30 and 55 zircon grains per sample were analyzed.

Isotopic disequilibria

The U–Th–Pb systematics of young rocks may be affected by disequilibrium partitioning of the intermediate daughter nuclides within the decay chain during crystallization of the mineral–isotopic system (Schmitz and Bowring 2001). All U–Th–Pb age calculations assume that all isotopes in the decay chain have attained secular equilibrium (i.e., all have equal numbers of decays per unit time). This means that any radioactive daughter isotope must be initially present in the mineral in amounts inversely proportional to their decay constant (Scharer 1984). However, enrichment or depletion of these intermediate daughter isotopes during crystallization can perturb the isotopic equilibrium of the decay chain (e.g., Barth et al. 1989).

In old samples (>100 Ma), the accumulation of radiogenic Pb effectively masks any effect of initial isotopic disequilibrium (Mattinson 1973). However, in young samples, sufficiently long-lived intermediate daughter products such as ^{230}Th and ^{234}U in the $^{238}U/^{206}Pb$ decay chain may dramatically affect the equilibrium systematics (Mattinson 1973; Scharer 1984).

Table 3 Summary of ELA-ICP-MS U-Pb isotopic ages for zircons in volcanic and subvolcanic units of the Farallón Negro Volcanics. All grid references are given as latitude and longitude, WGS 84

Intrusive phase	Sample	Longitude	Latitude	No. of analyses	Age[a] (Ma)	2σ	MSWD	No. of rejected zircons[b]	No. of inherited zircons	Th/U (rock)[c]	Age Th-corrected[c] (Ma)
Lower mafic to intermediate primary volcanic unit											
Basaltic andesite — Durazno Andesite	ACH00224	66°37′49.7″W	27°15′53.9″S	36	8.34	±0.14	1.27	9	13	5.20	8.46±0.14
	ACH00245	66°33′50.2″W	27°21′34.3″S	38	7.84	±0.27	2.49	8	22		7.94±0.27 [f]
Upper intermediate to silicic primary volcanic units											
Alumbrera Dacite	ACH9923	66°36′19.4″W[g]	27°19′56.1″S	45	7.89	±0.14	1.81	22	7	3.22	7.98±0.14
	ACHP2	N.D.[d]	N.D.	46	7.93	±0.14	1.67	9	16		8.02±0.14
La Josefe Tuff	ACH1083	66°37′25.3″W	27°18′55.4″S	46	7.96	±0.13	1.64	12	12	3.56	8.05±0.13
	ACH00297	66°40′3.5″W	27°16′22.6″S	46	7.87	±0.11	1.09	19	11		7.96±0.11
Dionisio Dacite	ACH1063	66°42′24.9″W	27°16′55.1″S	40	7.86	±0.17	2.48	12	13	4.40	7.95±0.17
Rhyolitic diatreme	ACH825	66°38′36.2″W	27°15′56.7″S	35	7.70	±0.13	1.30	9	11	3.84	7.79±0.13
Alto de la Blenda Andesite	ACH0056	66°38′42.2″W	27°19′7.4″S	38	7.28	±0.22	2.11	21	5	3.53	7.37±0.22
Agua Tapada Dacite	ACH1084	66°35′53.8″W	27°20′6.5″S	62	7.01	±0.07	1.59	15	0		7.10±0.07
	ACHLP3	N.D.[e]	N.D.	36	7.01	±0.07	1.81	2	0		7.10±0.07
	ACH1165	66°34′46.9″W	27°17′12.5″S	37	7.01	±0.06	1.02	11	0		7.10±0.06
	ACH755	66°34′56.0″W	27°17′11.5″S	47	6.92	±0.08	1.45	18	0		7.01±0.08
	ACH746	66°38′21.8″W	27°18′45.6″S	34	6.85	±0.08	1.00	12	0	3.22	6.94±0.08
	ACH00237	66°39′46.3″W	27°15′48.4″S	52	6.83	±0.07	1.61	14	2		6.93±0.07
Macho Muerto Rhyodacite	ACH1065	66°42′36.8″W	27°15′17.4″S	36	6.83	±0.07	1.21	10	0	3.45	6.92±0.07

[a]All uncertainties are 95% confidence limits
[b]Total number of excluded zircons on the basis of selection criteria presented in text
[c]^{230}Th corrected $^{206}Pb^*/^{238}U$ ratios. No extra uncertainty is attributed for this correction, which is minor
[d]Sample is from Diamond Drill Hole 49-60, 182 m at Bajo de la Alumbrera
[e]Sample is from Diamond Drill Hole 50.4-64.3, 625.5 m at Bajo de la Alumbrera
[f]Concordant criteria relaxed to allow enough data for age determination
[g] Sample collected from mine bench

During high temperature magmatic processes ^{234}U is not substantially fractionated from ^{238}U, such that only the ^{230}Th needs to be considered (Schmitz and Bowring 2001). The amount of ^{230}Th in a sample depends on the partition coefficient of the mineral calculated as $f=[Th/U]_{mineral}/[Th/U]_{magma}$, from the measured element concentrations (Schmitz and Bowring 2001). $[Th/U]_{mineral}$ was calculated from the mean measured Th and U concentration in each zircon analysis. The $[Th/U]_{magma}$ ratio was calculated using the measured concentration from bulk-rock samples determined with conventional ICP-MS (Table 3). Different rock types in the district range in Th and U concentration from 2 to 12 ppm and 0.5 to 3.5 ppm respectively, but the variation of the Th/U ratios is much smaller at 4.1±0.9 (n=8). All zircons analyzed are Th-deficient according to these $[Th/U]_{magma}$ values, with the magnitude of the ^{230}Th correction (i.e., ^{230}Th corrected) ranging from 80,000 to 100,000 years; i.e., ~1% age correction. The ^{230}Th disequilibrium-corrected $^{206}Pb^*/^{238}U$ isotopic ages for each sample are listed in Table 3. All $^{206}Pb/^{238}U$ age zircon ages reported for the Farallon Negro Volcanic Complex are the weighted means of ^{230}Th disequilibrium-corrected and 208-based common Pb-corrected $^{206}Pb/^{238}U$ ages (Table 3).

Late Miocene volcanism

Lower Basaltic Andesite and the Durazno Andesite

A clinopyroxene-phyric basaltic andesite monomictic breccia is the stratigraphically lowest zircon-bearing volcanic unit in the district. It occurs only 100 to 150 m from the base of the basaltic peperitic sills and lavas that form part of the Lower Basaltic Andesite (after Proffett 1997) and Durazno Andesite (Llambías 1972; Sasso 1997). The U–Pb zircon dates for two samples of the breccia unit are 8.46±0.14 to 7.94±0.27 Ma (Table 3; Fig. 6a). The latter zircon age is the most poorly determined age because of a relatively large common Pb component (Fig. 6b). Despite this, these ages are in good agreement with the hornblende $^{40}Ar/^{39}Ar$ ages reported by Sasso and Clark (1998) for the equivalent rocks (8.24±0.10, 8.37±0.10, and 8.59±0.10 Ma; Sasso 1997). In contrast, Sasso and Clark (1998) reported a 12.56±0.36 Ma (hornblende) age from a basaltic andesite unit (believed to be volcanic, but associated with intrusions) adjacent to the Bajo de la Alumbrera mine. The average of three separate total fusion ages, all of which are within analytical uncertainty, appears to define this age (Sasso 1997). Geologic mapping and section logging has confirmed that this 12.6 Ma unit lies stratigraphically above the 8.46±0.14 Ma old basaltic andesite monomictic breccia we report here (Harris 2002). Given this geologic context, the older age reported by Sasso and Clark (1998) may be due to excess Ar.

Subvolcanic and volcanic rocks of the Lower Basaltic Andesite contain a large population of 330 Ma zircons (25 out of 74 analyzed), more than other analyzed rocks in the Farallon Negro district. It is inferred that these magmas have assimilated or were partially melted from Paleozoic crystalline basement (e.g., Zentilli et al. 1994; Cornejo et al. 1997; Richards et al. 1999).

Alumbrera Dacite

This study has identified two discrete biotite-phyric dacite porphyry phases at Bajo de la Alumbrera deposit: one at ~8.0 Ma (Alumbrera Dacite, Proffett 1997; Ulrich and Heinrich 2001) and the other at ~7.0 Ma (Agua Tapada Dacite). Early mapping grouped these and all mineralized porphyries into the Agua Tapada Dacite subdivision (e.g., Llambías 1972). Given the age difference between phases, the term Alumbrera Dacite is applied here to the earliest porphyries at Bajo de la Alumbrera (i.e., P2 and Los Amarillos Porphyry). Petrographic studies combined with the geochronologic work confirm a cogenetic relationship of the regionally extensive phreatomagmatic deposits (referred to in this study as the La Josefe Tuff) with these dacitic porphyries. The phreatomagmatic deposits have ages of 8.05±0.13 and 7.96±0.11 Ma, whereas the Alumbrera Dacite porphyries have ages of 8.02±0.14 and 7.98±0.14 Ma (Table 3; Fig. 6c–f). This is the first time that magmatic (or crystallization) ages have been reported for the earliest porphyry phases at Bajo de la Alumbrera because, unlike $^{40}Ar/^{39}Ar$ isotopic ages of phenocrystic biotite or hornblende, zircons are able to retain their radiogenic daughter products even when subjected to pervasive hydrothermal alteration (Gebauer and Grunenfelder 1979; Cliff 1985) with temperatures of up to 650 °C (see fluid inclusion data for Bajo de la Alumbrera, Ulrich et al. 2001). These rocks also contain inherited zircons with ages of 9.0–9.8 and 11.7–12.7 Ma.

Dionisio Dacite

The uppermost volcanic member outcropping in the Farallon Negro district, termed the Dionisio Dacite, is a biotite-(plagioclase)-phyric dacite, which occurs as dykes, nested lava dome complexes, and autobreccias. Zircons from these rocks have a 7.95±0.17 Ma $^{206}Pb/^{238}U$ age (Table 3; Fig. 6g), so although being younger, the effusive eruption associated with these dacites are coeval with the explosive volcanism responsible for the regionally extensive phreatomagmatic deposits (La Josefe Tuff). However, during this time separating these two different eruption styles, exposure of the crystalline basement occurred, as evident from the abundance of boulder conglomerates and sandstones containing basement clasts that incise the tuffs. It is likely that, at the time when the Dionisio Dacite intruded, these sedimentary rocks were water-saturated, based on the spatial relationship to peperitic intrusions.

El Espanto and equivalent rhyolitic diatremes

There are several rhyolitic diatremes in the district, including the El Espanto diatreme south of Bajo de la Alumbrera (Fig. 2; Proffett 1997). Similar diatremes or breccia pipes are common along the Andes, notably Los Pelambres (Sillitoe 1973), Los Bronces-Rio Blanco (Stambuk et al. 1982; Warnaars et al. 1985) and El Teniente (Cuadra 1986), Chile, and Toquepala, Peru (Clark et al. 1990). The diatreme to the south of the Bajo las Pampitas porphyry Cu–Au occurrence is 7.79±0.13 Ma (Table 3; Fig. 6h). Its emplacement occurred during or immediately after uplift of the crystalline basement (i.e., 8.0–7.8 Ma), which in part is constrained by apatite fission-track cooling ages of adjacent Sierras Pampeanas (e.g., 7.6±2.2 Ma; Coughlin et al. 1998; Coughlin and Holcombe 2002). Skewes and Stern (1994) have proposed that similar breccias in the Frontal Cordillera are the result of a major uplift event that brought large water-saturated magma bodies to shallow depths, resulting in the explosive release of magmatic fluids. However, in the Farallón Negro district, the sedimentary succession was wet at the time of volcanism, as evident from the abundance of peperitic intrusions. As such, diatreme formation in the district could be a phreatomagmatic eruption caused through magma interacting with groundwater (e.g., Taupo, New Zealand; Wilson 1993).

Alto de la Blenda Andesite

The central Alto de la Blenda Andesite stock has a zircon $^{206}Pb/^{238}U$ age of 7.37±0.22 Ma (Table 3, Fig. 6i), which is within uncertainty of an $^{40}Ar/^{39}Ar$ age obtained from a sample of the same lithology collected at the same location, 7.50±0.20 Ma (hornblende) reported by Sasso and Clark (1998).

Agua Tapada Dacites

The biotite-phyric dacites assigned to the Agua Tapada Dacites are associated with alteration and mineralization, predominately within the porphyry centers at Bajo de la Alumbrera (e.g., Early and Late P3 porphyries, Ulrich and Heinrich 2001), but also Bajo el Durazno, Bajo Agua Tapada, and Bajo las Pampitas. Dykes that extend away from these deposits are commonly altered with varying amounts of secondary biotite–magnetite–quartz ± chlorite associated with minor Cu–Au–Mo. The U–Pb zircon ages for six samples of these rocks range from 7.10±0.07 to 6.93±0.07 Ma (Table 3, Fig. 6j–o). Excess argon and/or thermal resetting from subsequent hydrothermal events have probably affected some $^{40}Ar/^{39}Ar$ intrusion ages reported by Sasso and Clark (1998). As these are total fusion $^{40}Ar/^{39}Ar$ ages, this is difficult to demonstrate.

It is inferred that excess argon has strongly affected the $^{40}Ar/^{39}Ar$ intrusion ages from dacite porphyries at the subeconomic porphyry-related Cu–Au deposit, Bajo el Durazno. Sasso (1997) reports three ages that range from 8.33±0.18 to 8.20±0.11 Ma (hornblende) for the porphyries that have been potassically (biotite–K-feldspar–magnetite–quartz) altered. New U–Pb ages from the main and post mineralization porphyries at Bajo el Durazno are between 7.01±0.08 and 6.94±0.08 Ma (Table 3, Fig. 6j, m), making it younger than Bajo de la Alumbrera.

Macho Muerto Rhyodacite

The Macho Muerto Rhyodacite is the youngest intrusion in the district. These megacrystic sanidine rhyodacites have previously reported $^{40}Ar/^{39}Ar$ ages of 5.95±0.07 (biotite; Sasso 1997; Sasso and Clark 1998) and 6.91±0.25 Ma (whole rock; Sasso 1997), with the younger age being regarded as the true age — this is because of greater reproducibility of three individual total fusion ages and relatively low uncertainty (Sasso 1997). Mineral separates used in this younger age determination have acceptable K (r8.0 wt%) and low Ca concentrations, implying purity in the sample. New samples collected from the area originally analyzed yielded a U–Pb zircon age of 6.92±0.07 Ma (Table 3, Fig. 6p). Although the $^{40}Ar/^{39}Ar$ age could be recording the time at which the intrusion cooled through the biotite closure temperature (300 °C; McDougall and Harrison 1999), a million years is an unrealistically long time for a small intrusion to cool in a wet volcano-sedimentary pile. Despite the reproducibility of the fusion ages (Sasso 1997), Roberts et al. (2001) has shown that apparently pristine biotite can yield a disturbed age because of mineral breakdown during heating, and this may be the explanation of the young biotite age.

Zircon inheritance

In most samples, especially the oldest intrusions, there is inheritance of old zircons from the underlying crystalline basement. Morphologically these zircons are identical to the Late Miocene zircons; however, they yield U–Pb ages >200 Ma. Clearly most inherited zircons have an age of 330 Ma; however, they are as old as 1,100 Ma (Fig. 8). No old zircon has the very low Th/U (<0.01) characteristic of unarguably metamorphic grains. The oldest ages imply the existence of the Arequipa–Antofalla Craton (Lucassen et al. 2000) below the Farallón Negro Volcanic Complex. The outcropping crystalline basement comprises peraluminous and calc-alkaline syenogranites and monzogranites (Caelles 1979) and meta-siltstones and mudstones (Mirre and Acenolaza 1972). McBride et al. (1976) determined Ordovician K–Ar ages for the granites, which range from 423 to

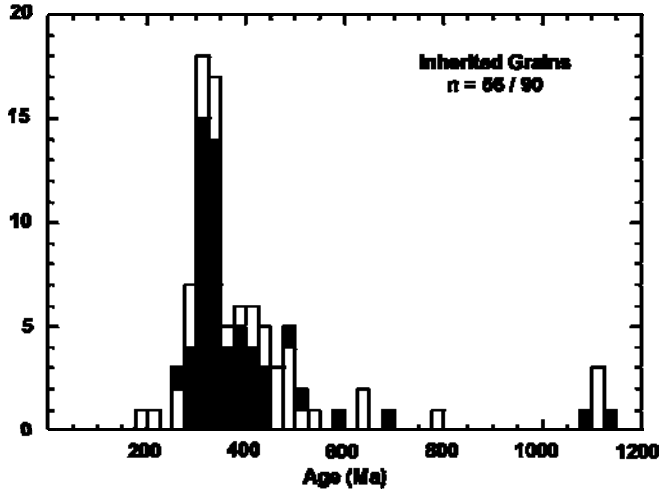

Fig. 8 Histogram of U–Pb data for unambiguously inherited zircons from all samples analyzed in this study. On the basis of the criteria outlined above, both the acceptable (filled boxes) data and rejected ages (open boxes) are plotted. These data were treated as all others except for those older zircons than 400 Ma, concordance is checked between $^{206}Pb/^{238}U$ and $^{207}Pb/^{206}Pb$. For those older than 800 Ma, the $^{207}Pb/^{206}Pb$ age is that reported

471 Ma, but more regionally within the Puna, major arc building occurred between 490 and 440 Ma, terminating with the Famatinian Stage of the Ocloyic Orogeny (Rapela et al. 1998). The ~330 Ma ages correspond to major back–arc magmatism associated with arc development in the Frontal Cordillera during the Variscan Stage (Damm et al. 1994).

Inherited Paleozoic zircon populations are common in mineralized porphyry Cu intrusions of South America (e.g., Zentilli et al. 1994; Cornejo et al. 1997; Richards et al. 1999). In spite of other radiogenic isotopic evidence that suggests minimal contamination by old crustal rocks (e.g., Tilton et al. 1981; Harmon et al. 1984; Pankhurst et al. 1988; Walker et al. 1991; Kay et al. 1999), the presence of these old zircons provides clear evidence of at least some crustal interaction in the generation of porphyry Cu magmas (Richards et al. 1999).

Associated hydrothermal alteration: a reassessment of earlier $^{40}Ar/^{39}Ar$ ages

The previously reported laser-probe $^{40}Ar/^{39}Ar$ incremental heating ages of phenocrystic biotite (i.e., 7.10±0.13, 6.98±0.08, and 6.83±0.07 Ma) from porphyries at Bajo de la Alumbrera were interpreted as an igneous event (Sasso 1997; Sasso and Clark 1998), but these samples occur in the potassic alteration zone. The description of the original sample material states that biotite occurs as coarse-grained phenocrysts and as fine-grained aggregates replacing hornblende. Sasso (1997) reported no evidence of recrystallization of the biotite phenocrysts. The young $^{40}Ar/^{39}Ar$ biotite age is from a sample with a low reported K (0.91 wt%) content and, therefore, is probably contaminated. Likewise, the other biotite samples have anomalously high Ca (~2.0 wt%) despite having more representative K concentrations (~8.0 wt%). Irrespectively, these two older biotite ages are based on three or more contiguous high-powered total fusion ages, demonstrating reproducibility (Sasso 1997). In light of the discrepancy with the U–Pb geochronology, we suggest that the $^{40}Ar/^{39}Ar$ ages of Sasso and Clark (1998) may, in part, represent the timing of potassic alteration.

Sasso and Clark (1998) have reported a $^{40}Ar/^{39}Ar$ age of 6.75±0.09 Ma (whole rock) for pervasive sericite alteration, slightly younger still than the biotite ages. It is probably a mixed age determination, as the whole-rock sample is from the innermost zone of pervasive phyllic alteration and overprints intermediate argillic assemblages. Here, all K-bearing silicate minerals (associated with earlier potassic alteration) are partially or entirely replaced very fine-grained illite (± chlorite).

Discussion

New U–Pb zircon geochronologic data, combined with a redefined volcanic stratigraphy of the Farallón Negro Volcanics, demonstrate the preservation of extrusive equivalents of the earliest dacitic intrusions in the Bajo de la Alumbrera porphyry Cu–Au deposit. Although Sillitoe (1973) was first to speculate on the cogenetic relationship between the volcanic rocks and the mineralized porphyritic intrusions, Proffett (1997) first described the Dionisio Dacite as the possible extrusive equivalents of the porphyritic intrusions at Bajo de la Alumbrera, and this study confirms those geologic observations. Sillitoe (1997) noted that three-quarters of known Au-rich porphyry Cu deposits are associated with coeval volcanic rocks; however, the majority of his examples are very young western Pacific deposits. The volcanic rocks adjacent to the Bajo de la Alumbrera deposit are unusual in South America, as Andean porphyry copper deposits generally lack coeval volcanic rocks (Camus 2002).

Temporal evolution of the Farallón Negro Volcanic Complex

New geochronologic constraints show that magmatism in the Farallón Negro district persisted for a little more than 1.5 million years (Fig. 9). The oldest preserved volcanism in the Farallón Negro Volcanic Complex began at about 8.5 Ma; however, older magmatism is implied in part by occurrence of 9.0–12.7 Ma xenocrystic zircons in subvolcanic intrusions throughout the district. In general, there is good agreement between the $^{40}Ar/^{39}Ar$ (Sasso and Clark 1998) and the U–Pb zircon ages, with the exception of a few older $^{40}Ar/^{39}Ar$ ages. Where significant discrepancies exist, they may be, in part, due to impurities or perhaps, more likely, excess Ar in the separates used in the $^{40}Ar/^{39}Ar$ geochronology

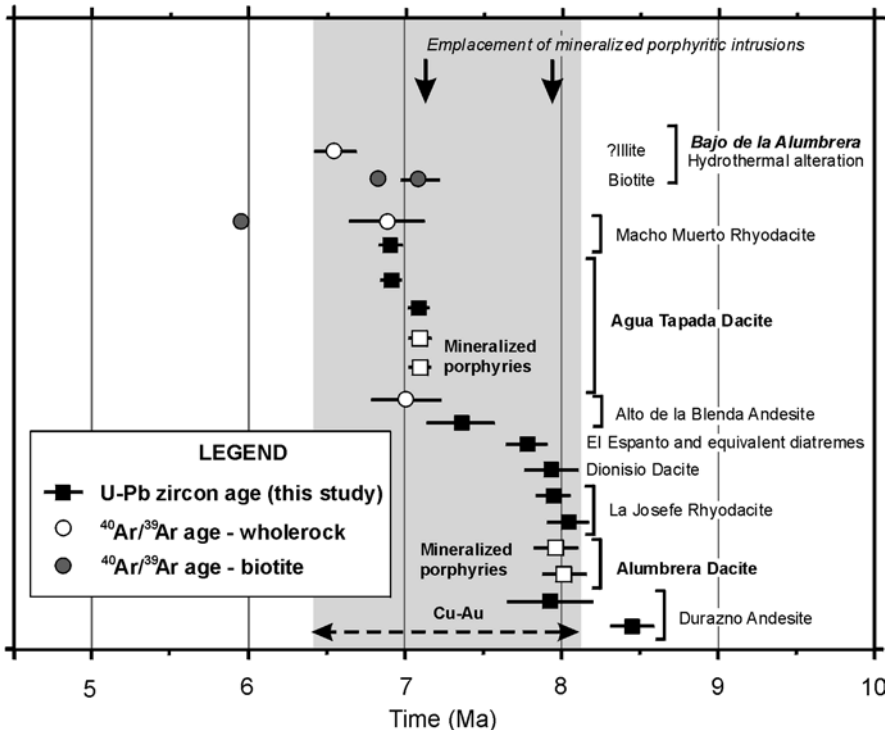

Fig. 9 The timing of intrusions in the Farallón Negro district. The duration of Cu–Au mineralization is constrained from the $^{40}Ar/^{39}Ar$ ages of Sasso and Clark (1998). Note that the timing of the diatremes follows erosion that would have unroofed the porphyry Cu–Au magmatic-hydrothermal system at Bajo de la Alumbrera. Renewed magmatism about a million years later was associated with the new Cu–Au mineralization in Bajo de la Alumbrera. The U–Pb age of the mineralized porphyries is highlighted by the open box symbols. The complete collapse of the regional magmatism soon followed, however, hydrothermal alteration may have continued

(e.g., Richards and McDougall 1990), or have an alternative geological meaning (e.g., the $^{40}Ar/^{39}Ar$ ages from phenocrystic biotite are probably the age of potassic alteration at Bajo de la Alumbrera).

The results of this study indicate that Late Miocene volcanism (and magmatism) in the Farallón Negro Volcanic Complex evolved from the early emplacement of mafic-intermediate lavas and subvolcanic intrusions at ~8.5 Ma (8.46±0.14 and 7.94±0.0.27 Ma), followed by multiple porphyritic intrusions related to episodic Cu–Au mineralization at Bajo de la Alumbrera, through to the final exposed subvolcanic intrusion by 6.8 Ma (6.92±0.07 Ma). The short duration of intrusive activity in the immediate Farallón Negro district differs from most Andean porphyry Cu provinces, whereby porphyry-related mineralization was emplaced episodically throughout extended regional igneous activity that can occur over tens of millions of years (Skewes and Stern 1995; Cornejo et al. 1997; Marsh et al. 1997). Alternatively, magmatism may have occurred at depth below Bajo de la Alumbrera, as suggested by the occurrence of inherited zircons with ages between 9.0 and 12.7 Ma.

Volcanism occurred in a siliciclastic intermontane basin, and represents the evolution of a multi-vent, flow-dome complex from early mafic to intermediate effusive phases (i.e., the lower lithofacies association, Table 1), to a silicic explosive phase, finally returning to an intermediate effusive phase with the waning of volcanism (i.e., the upper lithofacies association, Table 1). Early mafic volcanism at about 8.5 Ma consisted of subvolcanic intrusions and subaerial lava flows emanating from isolated centers throughout the basin. The source of the thick andesitic sedimentary breccias was the intrabasinal vents. Some volcanic detritus may have also been derived from more regional volcanic centers that developed before the Farallón Negro Volcanic Complex (see Rossello 1980).

Regionally extensive silicic explosive volcanism began at approximately 8.0 Ma and resulted in a thick succession of rhyolitic phreatomagmatic base surge and fallout deposits. These eruptions were probably centered on small volcanic edifices intruded into wet unconsolidated sediment causing phreatomagmatic eruptions. One such edifice occurred at Bajo de la Alumbrera, under which a weak, early Cu–Au-rich magmatic–hydrothermal system formed. The thickness of the early volcaniclastic stratigraphy (£ 650 m) and primary volcanic sills (100–500 m) to the base of the phreatomagmatic units (i.e., the lower mafic facies association) suggests that the depth of emplacement was very shallow (<1 km) at this time. Uplift and erosion soon followed, exposing parts of the crystalline basement and possibly resulted in unroofing of the earliest hydrothermal system. Small nested lava dome complexes were subsequently erupted, between which ephemeral lacustrine environments occurred. Late phreatomagmatic eruptions blanketed the district and occurred synchronously with the cessation of the first phase or cycle of magmatism within the district.

About 1.5 million years after the commencement of the volcanic complex, there was a renewed period of dacitic magmatism, and it is this magmatism that is associated with the bulk of the Cu–Au mineralization at Bajo de la Alumbrera. At about 7.1 Ma, a more substantial thickness of volcanic and volcaniclastic rocks was deposited over Bajo de la Alumbrera (i.e., the upper facies association). Pressure estimates from fluid

inclusions imply that the overburden of the system was ≈2.5 km (Ulrich et al. 2001; Harris 2002). At this time, the Alto de la Blenda Andesite intruded along with higher-level sills and dyke. This must have occurred immediately before emplacement of the dacitic porphyries at the other subeconomic mineralized centers of Bajo las Pampitas, Bajo el Durazno, and Bajo Agua Tapada. Finally, large flow-banded sills and dykes intruded the uppermost portions of the stratigraphy during waning of volcanism at approximately 6.8 Ma.

Reconstruction of the volcanic architecture has implications for the emplacement of porphyry Cu deposits. It can be demonstrated that the overburden confining the hydrothermal system at Bajo de la Alumbrera has fluctuated through time, with the earliest depths being <1 km and growing to ≈2.5 km during the main stages of mineralization. This later thickness is inferred from the occurrence of 6.9 Ma peperites in the upper parts of the preserved stratigraphy (Harris 2002). Previous volcanic models for the Farallón Negro district had the Bajo de la Alumbrera porphyry Cu–Au deposit positioned in the center or flank of a single large stratovolcano that attained heights up to 4 km (e.g., Sillitoe 1973; Proffett 1997). Stratigraphic relationships confirmed, by geochronologic data, the overall dominance of sedimentary facies, the recurrence of peperitic intrusions, the juxtaposition of proximal and more distal facies, and the cyclic changes in eruption styles and composition are more consistent with a multiple-vent eruptive complex in a large sedimentary basin.

Longevity of hydrothermal alteration

The combined duration of the intrusions and the associated hydrothermal alteration in several small- to medium-sized porphyry Cu deposits has been well documented (e.g., Divide, Silberman et al. 1979; Far Southeast-Lepanto, Arribas et al. 1995; Round Mountain, Henry et al. 1995; Potrerillos, Marsh et al. 1997). The longevity of these ore-forming hydrothermal systems is believed to be approximately equal to the resolving capabilities of the K–Ar and $^{40}Ar/^{39}Ar$ techniques (Hedenquist and Richards 1998), i.e., 100,000 to 300,000 years, and is consistent with the time required for the adjacent porphyritic stocks to cool (Elder 1977; Norton and Cathles 1979; Cathles 1981). By using a combination of $^{40}Ar/^{39}Ar$, K–Ar, Rb–Sr, and U–Pb isotopic systems as thermochronometers it is becoming possible to discriminate the intrusion age from the later hydrothermal alteration age. This approach suggests that a number of porphyry Cu deposits may have formed episodically over a few millions of years (e.g., Bajo de la Alumbrera, Argentina; Chuquicamata, El Salvador, and Escondida, Chile; Alpers and Brimhall 1988; Cornejo et al. 1997; Parry et al. 1997; Reynolds et al. 1998; Martin et al. 1999; Richards et al. 1999; Snee et al. 1999; Watanabe et al. 1999; Ballard et al. 2001; Mathur et al. 2000).

Our new data for Bajo de la Alumbrera show that the last known intrusion temporally related to hydrothermal alteration occurred at 7.10±0.07 Ma, and the last regional intrusive event was at 6.92±0.07 Ma. If taken at face value, the previously reported $^{40}Ar/^{39}Ar$ ages imply that hydrothermal alteration may have continued at least until 6.7 Ma. Although there is clear geochronologic evidence for multiple phases of intrusions in porphyry Cu deposits (e.g., Cornejo et al. 1997; Reynolds et al. 1998; Ballard et al. 2001), which confirm the geologic observations made by Lowell and Guilbert (1970), Sillitoe (1972), Gustafson and Hunt (1975), and many others, it appears that hydrothermal alteration can occur for much longer than is expected from heat flow modeling of a cooling intrusion (e.g., Norton and Knight 1977; Norton and Cathles 1979; Smith and Shaw 1979; Cathles 1981; Cathles et al. 1997). Such numerical models show that these small intrusions cannot solely sustain a hydrothermal system for much more than 100,000 years, let alone for a few to several hundred thousand years (e.g., Chuquicamata, Chile; Reynolds et al. 1998; Mathur et al. 2000). Resolution of this inconsistency requires more careful study of the cooling history of porphyry systems (e.g., McInnes et al. 1999).

Implications

The Bajo de la Alumbrera deposit resulted from the superposition of multiple porphyry-related hydrothermal systems, temporally separated by a million years. Similar relationships have been established at Chuquicamata, Chile (Ballard et al. 2001), which is a much larger porphyry Cu deposit (≈60 · 10^6 t of Cu) than Bajo de la Alumbrera (≈3 · 10^6 t of Cu). The concentration of metals in porphyry ore deposits is not simply a function of their longevity and/or the superposition of multiple porphyry systems (cf. Sillitoe 2000). Instead, the timing of processes operating in the parental magma body probably had a larger impact on the resultant hydrothermal systems, determining the volume and metal budget of the hydrothermal fluids evolved (e.g., Burnham 1967; Lowell and Guilbert 1970; Sillitoe 1972; Gustafson and Hunt 1975; Gustafson 1978; Beane and Titley 1981; Titley and Beane 1981; Titley 1982; Dilles and Einaudi 1992; Hedenquist et al. 1998).

Acknowledgements This project forms part of the first author's doctoral research at the University of Queensland, which was funded by an Australian Postgraduate Award scholarship. MIM Exploration and Minera Alumbrera are thanked for financial and logistical support and access to the Farallón Negro district. Mario Alderete from Yacimientos Mineros Agua de Dionisio (YMAD) is also thanked for granting initial access. The first author would like to thank the RSES for access to the ELA-ICP-MS and mineral separation facilities. SEM images were obtained with the help of Graeme Auchterlonie from the Centre for Microscopy and Microanalysis, the University of Queensland. Thanks are also due

to Rick Valenta, Steve Brown, John Proffett, Jim Dunlap, Ron Berry, Sue Keay, and David Keough and the many others who have been involved with the project. We thank Noel White for his insightful and thorough reviews of the manuscript resulting in substantial improvements. Richard Tosdal, Richard Goldfarb, Jeremy Richards and one other anonymous reviewer are acknowledged for their constructive comments that helped refine the manuscript.

References

Alpers CN, Brimhall GH (1988) Middle Miocene climatic change in the Atacama Desert, northern Chile; evidence from supergene mineralization at La Escondida. Geol So Am Bull 100:1640–1656

Arribas A Jr, Hedenquist JW, Itaya T, Okada T, Concepción RA, Garcia JS (1995) Contemporaneous formation of adjacent porphyry and epithermal Cu–Au deposits over 300 ka in northern Luzon, Philippines. Geology 23:337–340

Ballard JR (2001) A comparative study between the geochemistry of ore-bearing and barren calc-alkaline intrusions: PhD Thesis, Australian National University

Ballard JR, Palin JM, Williams IS, Campbell IH (2001) Two ages of porphyry intrusion resolved for the super-giant Chuquicamata copper deposit of northern Chile by ELA-ICP-MS and SHRIMP. Geology 29:383–386

Barth S, Oberli F, Meier M (1989) U–Th–Pb systematics of morphologically characterized zircon and allanite: a high-resolution isotopic study of the Alpine Rensen pluton (northern Italy). Earth Planet Sci Lett 95:235–254

Beane RE, Titley SR (1981) Porphyry copper deposits. Part II, Hydrothermal alteration and mineralization. In: Skinner BJ (ed) Econ Geol 75th anniversary volume; 1905–1980. Society of Economic Geologists Publication, pp 235–269

Black LP, Kamo SL, Williams IS, Foudoulis C, Claoué-Long JC, Korsch RJ, Davis DW (2000) The quest for a high-quality zircon standard for microbeam Pb–U–Th geochronology. Geol Soc Aust Abstr 59:43

Burnham CW (1967) Hydrothermal fluids at the magmatic stages. In: Barnes HL (ed) Geochemistry of hydrothermal ore deposits. Holt, Rinehart and Winston, New York, pp 34–76

Caelles JC (1979) The geological evolution of the Sierras Pampeanas Massif, La Rioja and Catamarca Provinces, Argentina. PhD Thesis, Queen's University

Caelles JC, Clark AH, Farrar E, McBride SL, Quirt S (1971) Potassium–argon ages of porphyry copper deposits and associated rocks in the Farallón Negro-Capillitas district, Catamarca, Argentina. Econ Geol 66:961–964

Camus F (2002) The Andean porphyry systems. In: Cooke DR, Pongratz J (eds) Giant ore deposits: characteristics, genesis and exploration. CODES Special Publication 4, Hobart, pp 5–22

Cathles LM (1981) Fluid flow and genesis of hydrothermal ore deposits. In: Skinner BJ (ed) Economic Geology 75th anniversary volume; 1905–1980. Society of Economic Geologists Publication, pp 424–457

Cathles LM, Erendi AHJ, Barrie T (1997) How long can a hydrothermal system be sustained by a single intrusive event? Econ Geol 92:766–771

Clark AH, Farrar E, Caelles JC, Haynes SJ, Lortie RB, McBride SL, Quirt GS, Robertson RCR, and Zentilli M (1976) Longitudinal variations in the metallogenetic evolution of the Central Andes; a progress report. In: Strong DF (ed) Special paper 14. Metallogeny and Plate Tectonics, Geological Association of Canada Special, pp 23–58

Clark AH, Tosdal RM, Farrar E, Plazolles VA (1990) Geomorphologic environment and age of supergene enrichment of the Cuajone, Quellaveco, and Toquepala porphyry copper deposits, southeastern Peru. Econ Geol 85:1604–1628

Cliff RA (1985) Isotopic dating of metamorphic belts. J Geol Soc Lond 142:97–110

Compston W, Williams IS, Meyer C (1984) U–Pb geochronology of zircons from lunar breccia 73217 using sensitive high mass-resolution ion microprobe. J Geophys Res 89(suppl):B525–B524

Cornejo P, Tosdal RM, Mpodozis C, Tomlinson AJ, Rivera O, Fanning CM (1997) El Salvador, Chile porphyry Copper deposit revisited: geologic and geochronologic framework. Int Geol Rev 39:22–54

Coughlin TJ, Holcombe RJ (2002) Linked faults and porphyry-skarn mineralization in the Central Andes. In: Vearncombe S (ed) Applied structural geology for mineral exploration and mining. Aust Inst Geosci Bull 36:36–38

Coughlin TJ, O'Sullivan PB, Kohn BP, Holcombe RJ (1998) Apatite fission-track thermochronology of the Sierras Pampeanas, central western Argentina; implications for the mechanism of plateau uplift in the Andes. Geology 26:999–1002

Cuadra P (1986) Geocronologia K–Ar del yacimiento El Teniente y areas adyacentes. Rev Geol Chile 27:3–26

Cumming GL, Richards JR (1975) Ore lead isotope ratios in a continuously changing earth. Earth Planet Sci Lett 28:155–171

Damm KW, Harmon RS, Kelley S (1994) Some isotopic and geochemical constraints on the origin and evolution of the Central Andean basement (19°)24°S). In: Reutter KJ, Scheuber E, Wigger PJ (eds) Tectonics of the southern Central Andes; structure and evolution of an active continental margin. Springer, Berlin Heidelberg New York, pp 263–276

Dawson SE (1994) The occurrence of gold at the Bajo de la Alumbrera porphyry copper–gold deposit, northwestern Argentina. MSc Thesis, University of Arizona

de Urreiztieta M, Gapais D, Le CC, Cobbold PR, Rossello E (1996) Cenozoic dextral transpression and basin development at the southern edge of the Puna Plateau, northwestern Argentina. Tectonophysics 254:17–39

Dilles JH, Einaudi MT (1992) Wall-rock alteration and hydrothermal flow paths about the Ann-Mason porphyry copper deposits, Nevada: a 6-km vertical reconstruction. Econ Geol 87:1963–2001

Durr S, Seide E, Kreuzer H, Harre W (1978) Témoins d'un metamorphisme d'age cretace superieur dans l'Egeide: dations radiometriques de mineraux provenant de l'ile de Nikouria (Cyclades, Grece). Bull Geol Soc France 20:209–213

Elder JW (1977) Model of hydrothermal ore genesis: Volcanic Studies Group of the Geological Society of London, 21–22 January 1976, Proceedings, pp 4–13

Gebauer D, Grunenfelder M (1979) U–Th–Pb dating of minerals. In: Jager E, Hunziker JC (eds) Lectures in isotope geology. Springer, Berlin Heidelberg New York, pp 101–131

Guilbert JM (1995) Geology, alteration, mineralization, and genesis of the Bajo de la Alumbrera porphyry copper–gold deposit, Catamarca province, Argentina. Arizona Geol Soc Dig 20:646–656

Gustafson LB (1978) Some major factors of porphyry copper genesis. Econ Geol 73:600–607

Gustafson LB, Hunt JP (1975) The porphyry copper deposit at El Salvador, Chile. Econ Geol 70:857–912

Godeas MC, Segal de Svetliza SJ (1980) Alteración hidrotermal y mineralización en el Bajo la Alumbrera, Provincia de Catamarca. Rev Asoc Geol Argentina 35:318–331

González OE (1975) Geología y alteración en el cobre porfídico ''Bajo la Alumbrera'': Rep. Argentina: II. Congreso Ibero-Americano de Geología Económica, pp 247–270

González Bonorino F (1950) Geologia y petrografia de las hojas 12d (Capillitas) y 13d (Andalgalá): Buenos Aires Direccion Nacional de Geologia y Mineria, Boletin

Harmon RS, Barreiro BA, Moorbath S, Hoefs J, Francis PW, Thorpe RS, Deruelle B, McHugh J, Viglino JA (1984) Regional O-, Sr-, and Pb-isotope relationships in Late Cenozoic calc-alkaline lavas of the Andean Cordillera. J Geol Soc Lond 141:803–822

Harris AC (2002) The genesis of a porphyry Cu–Au deposit, Farallón Negro Volcanic Complex, NW Argentina. PhD Thesis, University of Queensland

Hedenquist JW, Richards JP (1998) The influence of geochemical techniques on the development of genetic models for porphyry copper deposits. In: Richards JP, Larson PB (eds) Techniques in hydrothermal ore deposits geology. Rev Econ Geol 10:235–256

Hedenquist JW, Arribas A Jr, Reynolds TJ (1998) Evolution of an intrusion-centred hydrothermal system: far Southeast Lepanto porphyry and epithermal Cu–Au deposits, Philippines. Econ Geol 93:374–404

Henry CD, Elson HB, Castor SB (1995) Brief duration of hydrothermal activity at Round Mountain, Nevada, determined from $^{40}Ar/^{39}Ar$ geochronology. Geol Soc Am Abstr Programs 27:A329

Hirata T, Nesbitt RW (1995) U–Pb isotope geochronology of zircon: evaluation of the laser probe-inductively coupled plasma mass spectrometry technique. Geochim Cosmochim Acta 59:2491–2500

Horn I, Rudnick RL, McDonough WE (2000) Precise elemental and isotope ratio determination by simultaneous solution nebulization and laser ablation ICP-MS: Application to U–Pb geochronology. Chem Geol 164:281–301

Hwang IG, Chough SK, Hong SW, Choe NV (1995) Controls and evolution of fan delta systems in the Miocene Pohang Basin, SE Korea. Sediment Geol 98:147–179

Jordan TE, Allmendinger RW (1986) The Sierras Pampeanas of Argentina: a modern analogue of Rocky Mountain foreland deformation. Am J Sci 286:737–764

Jordan TE, Isacks BL, Allmendinger RW, Brewer JA, Ramos VA, Ando CJ (1983) Andean tectonics related to geometry of subducted Nazca Plate. Geol So Am Bull 94:341–361

Kay SM, Mpodozis C, Coira B (1999) Neogene magmatism, tectonism and mineral deposits of the Central Andes. In: Skinner BJ (ed) Geology and ore deposits of the Central Andes. Soc Econ Geol Spec Publ 7:27–59

Keay S (1998) The geological evolution of the Cyclades, Greece: constraints from SHRIMP U–Pb geochronology. PhD Thesis, Australian National University

Landtwing MR, Dillenbeck ED, Leake MH, Heinrich CA (2002) Evolution of the breccia-hosted porphyry Cu–Mo–Au deposit at Agua Rica, Argentina: progressive unroofing of a magmatic-hydrothermal system. Econ Geol 97:1273–1292

Lanphere MA, Baadsgaard H (2001) Precise K–Ar, $^{40}Ar/^{39}Ar$, Rb–Sr and U/Pb mineral ages from the 27.5 Ma Fish Canyon Tuff reference standard. Chem Geol 175:653–671

Llambías EJ (1972) Estructura del grupo volcanico Farallón Negro, Catamarca, República Argentina. Rev Asoc Geol Argentina 27:161–169

Lowell JD, Guilbert JM (1970) Lateral and vertical alteration-mineralization zoning in porphyry copper ore deposits. Econ Geol 65:373–408

Lucassen F, Becchio R, Wilke HG, Franz G, Thirlwall MF, Viramonte J, Wemmer K, (2000) Proterozoic–Paleozoic development of the basement of the Central Andes (18–26°S): a mobile belt of the South American craton. J S Am Earth Sci 13:697–715

Marsh TM, Einaudi MT, McWilliams M (1997) $^{40}Ar/^{39}Ar$ geochronology of Cu–Au and Au–Ag mineralization in the Potrerillos district, Chile. Econ Geol 92:784–806

Martin MV, Dilles JH, Proffett JM (1999) U–Pb geochronologic constraints for the Butte porphyry system. Geol Soc Am Abstr Programs 31:380

Mathur R, Ruiz J, Munizaga F (2000) Relationship between copper tonnage of Chilean base metal porphyry deposits and Os isotope ratios. Geology 28:555–558

Mattinson JM (1973) Anomalous isotopic composition of lead in young zircons. Carnegie Institute Washington Yearbook vol 72, pp 613–616

McBride SL, Caelles JC, Clark AH, Farrar E (1976) Paleozoic radiometric age provinces in the Andean basement, Latitudes 25°–30°S. Earth Planet Sci Lett 29:373–383

McDougall I, Harrison TM (1999) Geochronology and thermochronology by the $^{40}Ar/^{39}Ar$ method, 2 edn. Oxford University Press, New York

McInnes BIA, Farley KA, Sillitoe RH, Kohn BP (1999) Application of apatite (U–Th)/He thermochronometry to the determination of the sense and amount of vertical fault displacement at the Chuquicamata porphyry copper deposit, Chile. Econ Geol 94:937–948

Méndez V (1997) Yacimiento Bajo la Alumbrera, Provincia de Catamarca, República Argentina. Rev Asoc Argentina Geol Econ 11:15–30

Mirre JC, Acenolaza FG (1972) El hallazgo de Oldhamia sp. (traza fosil) y su valor como evidencia de edad Cambrica para el supuesto Precambrico del borde occidental del Aconquija, Prov de Catamarca. Ameghiniana 9:72–78

Norton D, Cathles LM (1979) Thermal aspects of ore deposits. In: Barnes HL (ed) Geochemistry of hydrothermal ore deposits, 2nd edn. Wiley, New York, pp 611–631

Norton D, Knight J (1977) Transport phenomena in hydrothermal systems: cooling plutons. Am J Sci 277:937–981

Pankhurst RJ, Hole MJ, Brook M (1988) Isotope evidence for the origin of Andean granites. Trans R Soc Edinb Earth Sci 79:123–133

Parry WT, Wilson PN, Jasumback MD, Heizler MT (1997) Clay mineralogy and $^{40}Ar/^{39}Ar$ dating of phyllic and argillic alteration at Bingham, Utah. Geol Soc Am Abstr Programs 29:282

Pearce NJG, Perkins WT, Westgate JA, Gorton MP, Jackson SE, Neal CR, Chenery SP (1997) A compilation of new and published major and trace element data for NIST SRM 610 and NIST SRM 612 glass reference materials. Geostand Newslett 21:115–144

Pe-Piper G, Kotopouli CN, Piper DJW (1997) Granitoid rocks of Naxos, Greece: regional geology and petrology. Geol J 32:153–171

Perelló J, Rojas N, Devaux C, Fava L, Etchart E Harman P (1998) Discovery of the Agua Rica porphyry Cu–Mo–Au deposit, Catamarca province, northwestern Argentina, Part II: geology. Australian Mineral Foundation Symposium, Perth, Western Australia, Proceedings, pp 117–132

Proffett JM (1995) Geology of the Bajo de la Alumbrera porphyry Cu–Au deposits, Catamarca Province, Argentina. Minera Alumbrera Ltd, Internal Report

Proffett JM (1997) Geology of the Bajo de la Alumbrera porphyry Cu–Au deposits, Catamarca Province, Argentina. Minera Alumbrera, Internal Report

Ramos VA, Reynolds JH, Jordan TE, Tabbutt KD (1988) Time constraints for the uplift of the Sierras de Toro Negro, Umango, and Espinal, western Sierras Pampeanas, Argentina. Geol Soc Am Abstr Programs 20:61

Rapela CW, Pankhurst RJ, Casquet C, Baldo E, Saavedra J, Galindo C, (1998) Early evolution of the Proto-Andean margin of South America. Geology 26:707–710

Reynolds JH, Tabbutt KT, Johnson NM, Jordan TE (1987) Non-systematic uplift of the northwestern Sierras Pampeanas, Catamarca Province, Argentina; interpretation of magnetic polarity stratigraphy data. Geol Soc Am Abstr Programs 19:817

Reynolds P, Ravenhurst C, Zentilli M, Lindsay D (1998) High-precision $^{40}Ar/^{39}Ar$ dating of two consecutive hydrothermal events in the Chuquicamata porphyry copper system, Chile. Chem Geol 148:45–60

Richards JP, McDougall I (1990) Geochronology of the Porgera gold deposit, Papua New Guinea: resolving the effects of excess argon on K–Ar and $^{40}Ar/^{39}Ar$ age estimates for magmatism and mineralization. Geochim Cosmochim Acta 54:1397–1415

Richards JP, Noble SR, Pringle MS (1999) A revised Late Eocene age for porphyry Cu magmatism in the Escondida Area, Northern Chile. Econ Geol 94:1231–1248

Roberts HJ, Kelley SP, Dahl PS (2001) Obtaining geologically meaningful $^{40}Ar–^{39}Ar$ ages from altered biotite. Chem Geol 172:277–290

Rojas N, Perelló J, Harman P, Cabello J, Devaux C, Fava L, Etchart E (1998) Discovery of the Agua Rica porphyry Cu–Mo–Au deposit, Catamarca province, northwestern

Argentina, Part I: exploration and discovery. Australian Mineral Foundation Symposium, Perth, Western Australia, Proceedings, pp 111–117

Rossello EA (1980) Nuevo complejo volcanico Vicuna Pampa, Departamento Belen, Provincia de Catamarca. Rev Asoc Geol Argentina 35:436–438

Sasso AM (1997) Geological evolution and metallogenetic relationships of the Farallón Negro volcanic complex, NW Argentina. PhD Thesis, Queens University

Sasso AM, Clark AH (1998) The Farallón Negro group, northwest Argentina: magmatic, hydrothermal and tectonic evolution and implications for Cu–Au metallogeny in the Andean back-arc. Soc Econ Geol Newslett 34(1):8–18

Scharer U (1984) The effect of initial ^{230}Th disequilibrium on young U–Pb ages: the Makalu case, Himalaya. Earth Planet Sci Lett 67:191–204

Schmitz MD, Bowring SA (2001) U–Pb zircon and titanite systematics of the Fish Canyon Tuff: an assessment of high-precision U–Pb geochronology and its application to young volcanic rocks. Geochim Cosmochim Acta 65:2571–2587

Silberman ML, Bonham HF Jr, Garside LJ, Ashley RP (1979) Timing of hydrothermal alteration-mineralization and igneous activity in the Tonopah mining district and vicinity, Nye and Esmeralda Counties, Nevada. Nevada Bur Mines Geol Report 33:119–126

Sillitoe RH (1972) A plate tectonic model for the origin of porphyry copper deposits. Econ Geol 67:184–197

Sillitoe RH (1973) The tops and bottoms of porphyry copper deposits. Econ Geol 68:799–815

Sillitoe RH (1997) Characteristics and controls of the largest porphyry copper–gold and epithermal gold deposits in the circum-Pacific region. Aust J Earth Sci 44:373–388

Sillitoe RH (2000) Gold-rich porphyry deposits: descriptive and genetic models and their role in exploration and discovery. In: Hagemann SG, Brown PE (eds) Gold in 2000. Rev Econ Geol 13:315–345

Sister RG (1963) Informe geológico-económico de Farallón Negro y zona adyacente, Distrito Haulfin, Departamento Belen, Provincia de Catamarca, Opera Lilloana, VIII

Skewes MA, Stern CR (1994) Tectonic trigger for the formation of Late Miocene Cu-rich megabreccias in the Andes of central Chile. Geology 22:551–554

Skewes MA, Stern CR (1995) Genesis of the giant Late Miocene to Pliocene copper deposits of central Chile in the context of Andean magmatic and tectonic evolution. Int Geol Rev 37:893–909

Smalley R (1996) Andean crustal and upper mantle structure in the thick-skinned Sierras Pampeanas of San Juan, Argentina. Geol Soc Am Abstr Programs 28:112

Smith RL, Shaw HR (1979) Igneous-related geothermal systems. US Geol Surv Circ 790:12–17

Snee L, Miggins D, Geissman JW, Reed MH, Dilles JH, Zhang L (1999) Thermal history of the Butte porphyry system, Montana. Geol Soc Am Abstr Programs 31:380

Stambuk V, Blondel J, Serrano L (1982) Geologia del yacimiento Rio Blanco. Congr Geol Chileno Actas 2:E419–E442

Stults A (1985) Geology of the Bajo de la Alumbrera porphyry copper and gold prospect, Catamarca Province, Argentina. MSc Thesis, University of Arizona

Strecker MR, Cerveny P, Bloom AL, Malizia D (1989) Late Cenozoic tectonism and landscape development in the foreland of the Andes; northern Sierras Pampeanas (26°–28°S), Argentina. Tectonics 8:517–534

Strecker MR, Bloom AL, Malizia D (1990) Neotectonic activity in the northern Sierras Pampeanas, Argentina: Colloques et Seminaires. Institut de Recherche Scientifique pour le Developpement en Cooperation, Paris, pp 99–102

Tabbutt KD (1990) Temporal constraints on the tectonic evolution of Sierra de Famatina, northwestern Argentina, using the fission-track method to date tuffs interbedded in synorogenic clastic sedimentary strata. J Geol 98:557–566

Tabbutt K, Naeser CW, Jordan TE, Cerveny PF (1987) Edades nuevas por metodo de trazas de fision de todas Mio-Pliocene en las sierras Pampeanas y la Precordillera de Argentina. Actas Congr Geol Argentino 4:222–224

Tilton GR, Pollak RJ, Clark AH, Robertson RCH (1981) Isotopic composition of Pb in central Andean ore deposits. Geol Soc Am Mem 154:791–816

Titley SR (1982) The style and progress of mineralization and alteration in porphyry copper systems. In: Titley SR (ed) Advances in geology of the porphyry copper deposit, southwestern North America. University of Arizona Press, Tucson, pp 93–116

Titley SR, Beane RE (1981) Porphyry copper deposits; part I, geologic settings, petrology, and tectogenesis. In: Skinner BJ (ed) Economic Geology 75th Anniversary Volume; 1905–1980. Society of Economic Geologists Publication, pp 214–235

Ulrich T, Heinrich CA (2001) Geology and alteration geochemistry of the porphyry Cu–Au deposit at Bajo de la Alumbrera, Argentina. Econ Geol 96:1719–1742

Ulrich T, Gunthur D, Heinrich CA (2001) The evolution of a porphyry Cu–Au deposit, based on LA-ICP-MS analysis of fluid inclusions: Bajo de la Alumbrera, Argentina. Econ Geol 96:1743–1774

Walker JA, Moulds TN, Zentilli M, Feigenson MD (1991) Spatial and temporal variations in volcanics of the Andean Central Volcanic Zone (26 to 28°S). Geol Soc Am Spec Pap 265:139–155

Warnaars FW, Holmgren C, Barassi S (1985) Porphyry copper and tourmaline breccias at Los Bronces-Rio Blanco, Chile. Econ Geol 80:1544–1565

Watanabe Y, Stein HJ, Morgan JW, Markey RJ (1999) Re–Os geochronology brackets timing and duration of mineralization for the El Salvador porphyry Cu–Mo deposit, Chile. Geol Soc Am Abstr Programs 31:30

Watson EB, Cherniak DJ, Hanchar JM, Harrison TM, Wark DA (1997) The incorporation of Pb into zircon. Chem Geol 141:19–31

Wijbrans JR, McDougall I (1988) Metamorphic evolution of the Attic Cycladic Metamorphic Belt on Naxos (Cyclades, Greece) utilizing ^{40}Ar/^{39}Ar age spectrum measurements. J Metamorph Geol 6:571–594

Wilson CJN (1993) Stratigraphy, chronology, styles and dynamics of late Quaternary eruptions from Taupo Volcano, New Zealand. Phil Trans R Soc Lond, Phys Sci Eng 343:205–306

Zentilli M, Krogh TE, Maksaev V, Alpers CN (1994) Uranium-lead dating of zircons from the Chuquicamata and La Escondida porphyry copper deposits, Chile: inherited zircon core of Paleozoic age with Tertiary overgrowths. Comunicaciones 45:101–110